Forschungszentrum Jülich
in der Helmholtz-Gemeinschaft

Beam-Target Interaction and Intrabeam Scattering in the HESR Ring: Emittance, Momentum Resolution and Luminosity

Studie im Auftrag des Instituts für Kernphysik des Forschungszentrums Jülich GmbH

Frank Hinterberger

(Helmholtz-Institut für Strahlen- und Kernphysik der Universität Bonn, Deutschland)

Jül-4206

Beam-Target Interaction and Intrabeam Scattering in the HESR Ring: Emittance, Momentum Resolution and Luminosity

Studie im Auftrag des Instituts für Kernphysik des Forschungszentrums Jülich GmbH

Frank Hinterberger

(Helmholtz-Institut für Strahlen- und Kernphysik der Universität Bonn, Deutschland)

Berichte des Forschungszentrums Jülich ; 4206
ISSN 0944-2952

Zu beziehen durch: Forschungszentrum Jülich GmbH · Zentralbibliothek
D-52425 Jülich · Bundesrepublik Deutschland
☎ 02461 61-5220 · Telefax: 02461 61-6103 · e-mail: zb-publikation@fz-juelich.de

Strahl-Target Wechselwirkung und Intrabeam Scattering in dem HESR Ring: Emittanz, Impulsauflösung und Luminosität

Zusammenfassung

Die Strahl-Target Wechselwirkung wird im Hinblick auf die Zunahme der transversalen und longitudinalen Emittanz des Antiprotonenstrahls im HESR Speicherring untersucht. Das transversale Emittanzwachstum, das durch die Kleinwinkelstreuung verursacht wird, kann mit Hilfe des differentiellen Wirkungsquerschnitts der Coulomb Streuung analytisch beschrieben werden. Ebenso kann das longitudinale Emittanzwachstum, das durch den Energieverlust des Strahls verursacht wird, mit Hilfe des auf den Energieverlust bezogenen differentiellen Wirkungsquerschnitts berechnet werden. Es wird gezeigt, dass Teilchen, die einen Energieverlust in der Nähe des maximal möglichen Energieverlustes bei einem frontalen Stoss mit einem Targetelektron erleiden, wegen der eingeschränkten Impulsakzeptanz des HESR Rings verloren gehen. Die Annahme einer relativen Impulsakzeptanz von $1 \cdot 10^{-3}$ ergibt eine um eine Größenordnung kleinere Wachstumsrate der mittleren quadratischen Impulsabweichung. Die für den High Resolution Mode und High Luminosity Mode notwendigen Kühlraten werden unter der Annahme berechnet, dass die Aufheizung des Strahls durch die Strahl-Target Wechselwirkung dominiert wird. Zum Vergleich werden die Intrabeam-Scattering Effekte abgeschätzt. Sowohl für die Elektronenkühlung wie für die stochastische Kühlung werden analytische Ausdrücke angegeben, die zur Berechnung der Kühlraten und der erreichbaren Impulsauflösung verwendet werden können. Das Potential der Elektronenkühlung und der stochastischen Kühlung wird im Hinblick auf die erreichbare Impulsauflösung und den Strahl-Target Überlapp diskutiert. Strahlverlustraten und über die Zeit gemittelte Luminositäten werden berechnet. Dabei werden der totale hadronische Wirkungsquerschnitt, die eingeschränkte Impulsakzeptanz des HESR Rings, die Großwinkelstreuung der Coulomb Wechselwirkung und der Touschek Effekt berücksichtigt.

Beam-Target Interaction and Intrabeam Scattering in the HESR Ring: Emittance, Momentum Resolution and Luminosity

Abstract

The beam-target interaction is studied with respect to the transverse and longitudinal emittance growth of the HESR antiproton beam. The transverse emittance growth caused by the small angle Coulomb scattering can be described analytically using the differential cross section of the Coulomb interaction. Similarly, the longitudinal emittance growth caused by the energy loss of the beam can be calculated using the differential cross section of the energy-loss distribution. It is shown that particles with energy losses near the maximum energy loss in a head-on collision with a target electron are lost due to momentum acceptance of the HESR ring. Taking a relative momentum acceptance of about $1 \cdot 10^{-3}$ into account yields an order of magnitude smaller growth rate of the mean square momentum deviation. The necessary cooling rates for the High Resolution mode and the High Luminosity mode are deduced assuming that the beam-target interaction is the dominant beam heating process. For comparison the effects of intrabeam scattering are estimated. For electron and stochastic cooling, analytic expressions are quoted in order to evaluate the momentum resolution and cooling rate. The potentialities of electron and stochastic cooling are discussed with respect to the achievable momentum resolution and beam-target overlap. Beam loss rates and average luminosities are evaluated taking the total hadronic cross section, the restricted momentum acceptance of the HESR ring, the large angle Coulomb scattering and the Touschek effect into account.

1. Introduction

The High-Energy Storage Ring (HESR) of the future International Facility for Antiprotons and Ion Research (FAIR) at GSI in Darmstadt is designed as synchrotron and storage ring for antiprotons in the momentum range 1.5 – 15 GeV/c [1, 2]. Internal target experiments with antiprotons are planned by the PANDA collaboration [3]. In addition two other collaborations (PAX [4, 5], ASSIA [6]) proposed spin physics experiments with polarized antiprotons. In the present work the effects of the beam-target interaction, especially the beam heating effects, are studied in view of the required cooling rates, momentum resolution, luminosity and beam lifetime.

Two modes of operation are foreseen for the internal target experiment PANDA at the HESR. In the High Resolution (HR) mode $1 \cdot 10^{10}$ antiprotons are stored with a relative momentum spread in the order of 10^{-5}. In the High Luminosity (HL) mode up to $1 \cdot 10^{11}$ antiprotons can be stored with a relative momentum spread of about $1 \cdot 10^{-4}$. The effective target thickness of the internal hydrogen target is $4 \cdot 10^{15}$ atoms/cm^2 and the revolution frequency is about 0.52 MHz. The original design aims for luminosities of $2 \cdot 10^{31}$ cm^{-2}s^{-1} for the HR mode and $2 \cdot 10^{32}$ cm^{-2}s^{-1} for the HL mode. In the following, the *standard mode of operation* for HR and HL refers to equilibrium emittances[1] $\epsilon_{eq} = 1$ mm mrad, maximum scattering angles $\Theta_{cut} = 4$ mrad, transverse acceptances of 16 mm mrad and a relative momentum acceptance $\delta_{cut} = 1 \cdot 10^{-3}$.

In order to evaluate the beam heating by the beam-target interaction and the necessary cooling rates the transverse and longitudinal emittance growth is deduced analytically. The transverse emittance growth is determined by the differential cross section of the small angle Coulomb scattering between antiprotons and target nuclei. The longitudinal emittance growth, i.e. the growth of the mean square momentum deviation is determined by the energy straggling of the beam-target interaction. It can be derived from the differential cross section of the Coulomb interaction between antiprotons and target electrons. The energy straggling depends linearly on the maximum energy loss in a head-on collision with a target electron. At HESR energies the maximum energy losses are very high (e.g. 90 MeV at 8.0 GeV). Restricting the energy loss by adjusting the relative momentum acceptance of the ring to about $1 \cdot 10^{-3}$ yields an order of magnitude smaller growth rate of the mean square momentum deviation.

The study of the beam-target effects includes a comparison with other beam-heating processes. Especially, the effects of intra-beam scattering are calculated and compared with the beam-target interaction. In addition the potentialities of electron cooling and stochastic cooling are studied with respect to the achievable cooling rates.

An important point of the study is the investigation of beam losses. The main beam losses are caused by (i) the total cross section of the hadronic interaction between the antiprotons and the target protons, (ii) the restricted momentum acceptance of the ring, (iii) the integrated cross section of the large angle Coulomb scattering in the target, and (iv) the intrabeam scattering, especially the socalled Touschek effect.

2. Transverse Emittance Growth

The transverse emittance growth due to an internal target can be described analytically. For a derivation of the formulas we refer to ref. [8].

The HESR lattice is designed such that the betafunctions β_x and β_y are rather small at the position of the internal target. In addition, the periodic dispersion is zero, i.e. $D = 0$ and $D' = 0$. Therefore, the transverse emittance growth can be described by

$$\Delta\epsilon_{x,y} = \frac{1}{2}\beta_{x,y}\Theta^2_{rms}. \tag{1}$$

[1]The beam emittance is denoted by the symbol ϵ. Our definition of ϵ is such that the full emittance area is given by $E = \pi\epsilon$. Thus, our definition of the beam emittance ϵ and the machine acceptance ϵ_{acc} is without the factor π.

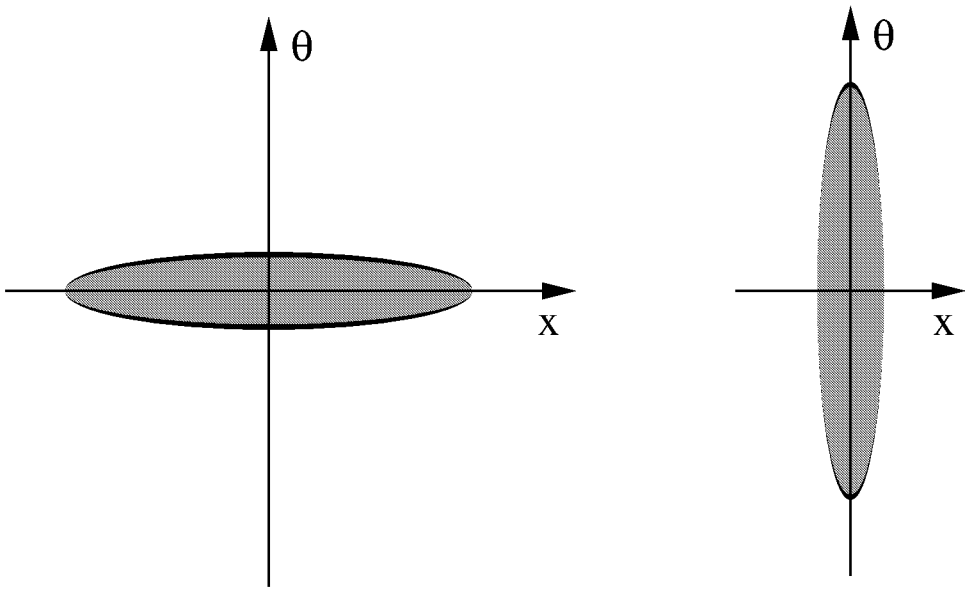

Fig. 1: Emittance growth (dark band) per target traversal. Left: large value of β_x. Right: small value of β_x.

Here, $\Delta\epsilon_{x,y}$ is the transverse emittance growth per turn in x and y direction, respectively and Θ^2_{rms} the mean square scattering angle per target traversal.

Without cooling the rate of transverse emittance growth is given by

$$\frac{\mathrm{d}\epsilon_{x,y}}{\mathrm{d}t} = \frac{1}{2}\beta_{x,y}\Theta^2_{rms}f. \tag{2}$$

Here, f is the revolution frequency of the internal beam. As a consequence, the emittance increases linearly with time t,

$$\epsilon_{x,y}(t) = \epsilon_{x,y}(0) + \frac{1}{2}\beta_{x,y}\Theta^2_{rms}ft, \tag{3}$$

as long as the emittance growth is not stopped by the ring acceptance, beam scrapers and/or beam cooling processes.

A pictorial representation of the emittance growth per target traversal is shown in Fig. 1 taking the horizontal phase ellipse as an example. The phase ellipse represents the beam density distribution corresponding to one standard deviation in x and Θ. Here, x is the horizontal position and Θ the horizontal angle with respect to the reference particle. The difference between the left and right ellipse is the magnitude of the betafunction at the target. The left phase ellipse is characterized by a relatively large value of β_x, the right by a relatively small value.

The effect of emittance growth is due to the mean square scattering angle Θ^2_{rms} of the small angle Coulomb scattering in the target. The corresponding rms width Θ_{rms} is added quadratically to the existing rms width Θ^{beam}_{rms} of the beam. The resulting distortion is shown as two dark bands. They move around the ellipse according to the betatron phase advance per turn and new distortions are added quadratically turn by turn. The factor 1/2 in Eq. (1) is a consequence of the fact that the phase ellipse is growing continuously in x and Θ.

Comparing the left and right ellipses shows intuitively that the emittance growth is directly proportional to the value of the betafunction at the target (see Eq. (1)). Therefore, the emittance growth can be kept small by designing a lattice with small values of β_x and β_y at the target.

2.1 Small angle Coulomb scattering and determination of Θ^2_{rms}

In principle, the mean square angle Θ^2_{rms} of the small angle multiple scattering is the second moment of a probability density distribution. Much theoretical effort [7] has been spent to predict the evolution of the *plural* and *multiple* Coulomb scattering distributions which are characterized by a Gaussian peak and long tails which tend approximately to the single scattering distributions at larger angles. Fortunately it is not necessary to know the details of the *plural* and *multiple* scattering distributions, since for any distribution the mean square value is just the mean-square *single* scattering angle multiplied by the mean number of scatterings [8]. We neglect all projectile-target interactions other than the Coulomb interaction. We assume fully stripped ions and high velocities ($\beta \gg Z_1/137$). In the following we quote the formulas which have been established in [8]. The quantity Θ^2_{rms} is obtained from the Rutherford cross section by calculating the mean square value α^2_{rms} of the spatial angle distribution in small angle approximation,

$$\alpha^2_{rms} = N_t z_{eff} \int_{\alpha_1}^{\alpha_2} \alpha^2 \left(\frac{Z_1 Z_2 e^2}{2\pi\epsilon_0 p\beta c} \right)^2 \frac{1}{\alpha^4} 2\pi\alpha \mathrm{d}\alpha, \tag{4}$$

Here, $N_t z_{eff}$ is the effective number of target atoms/cm^2 and Z_1 and Z_2 denote the target and projectile charge number. This equation yields

$$\alpha^2_{rms} = N_t z_{eff} 2\pi \left(\frac{Z_1 Z_2 e^2}{2\pi\epsilon_0 p\beta c} \right)^2 \ln\left(\frac{\alpha_2}{\alpha_1}\right). \tag{5}$$

It should be noted that Θ^2_{rms} is the mean square value of the plane projected distribution, thus for reasons of symmetry

$$\Theta^2_{rms} = \frac{1}{2}\alpha^2_{rms}. \tag{6}$$

The upper integration constant in Eq. (5) is determined by the De Broglie wavelength $\lambda/(2\pi) = \hbar/p$ and the nuclear radii of target and projectile,

$$\alpha_2 = \frac{\lambda/(2\pi)}{(A_1^{1/3} + A_2^{1/3})r_0}. \tag{7}$$

Here, A_1 and A_2 are the mass numbers of target and projectile. For the Coulomb interaction between proton and antiproton we take the nuclear charge radius of the proton, $r_0 = 0.870$ fm [9]. The lower integration constant is determined by the screening of the atomic electrons. Taking the Fermi screening radius a

$$a = 0.885 a_0 (Z_1^{2/3} + Z_2^{2/3})^{1/2} \tag{8}$$

where Z_1 and Z_2 are the charge numbers of projectile and target and a_0 the Bohr radius ($a_0 = 0.529 \cdot 10^{-8}$ cm) one has approximately

$$\alpha_1 = \frac{\lambda/(2\pi)}{a}. \tag{9}$$

This estimate can be improved by using Molière's formula for screened ion-atom potentials [10, 11] of the Thomas-Fermi type, i.e. by replacing the expression $\ln(\alpha_2/\alpha_1)$ in Eq. (5) by

$$\ln\left(\frac{\alpha_2}{\alpha_1}\right) \to \frac{1}{2}\left[\ln\left(\frac{\alpha_2^2}{\chi^2}\right) - 1\right], \tag{10}$$

where the screening angle χ is given by

$$\chi^2 = 1.13\,\alpha_1^2 \left[1 + 3.33\left(\frac{Z_1 Z_2}{137\,\beta}\right)^2\right]. \tag{11}$$

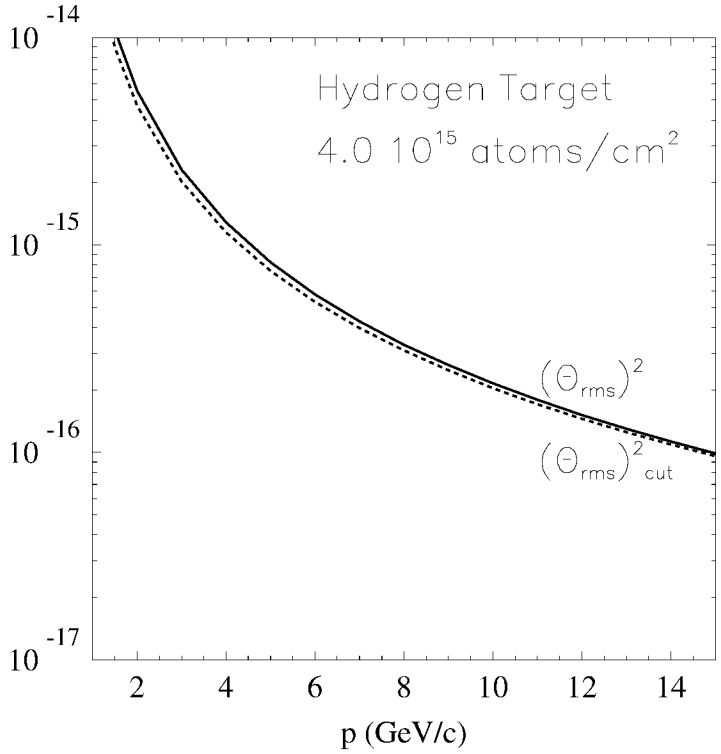

Fig. 2: Mean square scattering angle Θ^2_{rms} and $\Theta^2_{rms,cut}$ with $\Theta_{cut} = 4$ mrad vs. beam momentum p.

Molière's theory was further advanced by Fano [12] who considered the contribution of inelastic collisions with atomic electrons. This effect is taken into account by adding a corrective term Δb,

$$\Delta b = \frac{1}{Z_2}\left\{\ln\left[\frac{1130\,\beta^2}{Z_2^{4/3}(1-\beta)^2}\right] - u_{in} - \frac{\beta^2}{2}\right\}. \tag{12}$$

Here, u_{in} is a constant determined by the electron configuration of the target atom. For the hydrogen atom an exact calculation yields $u_{in} = -3.6$. Taking Molière's theory with Fano's modification the final formula for Θ^2_{rms} reads

$$\Theta^2_{rms} = \frac{1}{2} N z_{eff} \pi \left(\frac{Z_1 Z_2 e^2}{2\pi\epsilon_0 p\beta c}\right)^2 \left[\ln\left(\frac{\alpha_2^2}{\chi^2}\right) - 1 + \Delta b\right], \tag{13}$$

where α_2 is given by Eq. (7) and χ^2 by Eq. (11).

A simple approximation yields

$$\Theta^2_{rms} = \left(\frac{14.1\ \text{MeV}}{p\beta c}\right)^2 \frac{z_{eff}}{L_{rad}}. \tag{14}$$

Here, p is the beam momentum, βc the beam velocity, z_{eff} the effective target thickness in z direction and L_{rad} the corresponding radiation length. This equation has been derived by Rossi and Greisen [13]. The usefulness of Eq. (14) is due to the fact that the quantity $1/L_{rad}$ has a similar A and Z dependence as Θ^2_{rms}. Eq. (14) is also reported by the particle data group [9] but with a thickness dependent correction factor $[1 + 0.038\ln(z_{eff}/L_{rad})]$. The idea of the correction factor is to take only the central 98 % of the angular distribution into account. However, the contributions from the low intensity single scattering

tails of the angular distribution cannot be neglected because of the large number of target traversals. Therefore, the thickness dependent correction factor *must be omitted.*

For an antiproton beam of 9 GeV/c and a hydrogen target of $4 \cdot 10^{15}$ atoms/cm^2 Eq. (13) yields

$$\Theta^2_{rms} = 2.64 \cdot 10^{-16}. \tag{15}$$

The approximation of Eq. (14) yields $\Theta^2_{rms} = 2.76 \cdot 10^{-16}$ in fair agreement with the value of Eq. (15). In Fig. 2 the mean square scattering angle Θ^2_{rms} according to Eq. (13) is plotted as a function of the beam momentum for a hydrogen target with an effective target thickness of $4 \cdot 10^{15}$ atoms/cm^2.

2.2 Restricted small angle Coulomb scattering

However, inspecting the formulas for the calculation of Θ^2_{rms}, it turns out that *the maximum scattering angle is too large* in the HESR momentum range from 1.5 – 15 GeV/c.

Now, we calculate the effect of replacing the maximum scattering angle α_2 in Eq. (13) by an upper scattering angle $\alpha_{cut} = \Theta_{cut}$ which is defined by the finite acceptance ϵ_{acc} of the HESR ring

$$\alpha_{cut} = \Theta_{cut} = \sqrt{\frac{\epsilon_{acc}}{\beta_{x,y}}}. \tag{16}$$

The acceptance ϵ_{acc} defines the upper limit of the beam emittance and β_x and β_y are the values of the betafunction at the target point. Assuming $\beta_{x,y} = 1$ m and $\epsilon_{acc} = 16$ mm mrad yields as a typical value

$$\alpha_{cut} = \Theta_{cut} = 4 \text{ mrad}. \tag{17}$$

This value is much smaller than the maximum scattering angles α_2. However, the change of Θ^2_{rms} is

Table 1: Θ^2_{rms} for maximum and restricted scattering angle α_2 and $\alpha_{cut} = \Theta_{cut} = 4$ mrad, respectively.

p (GeV/c)	Δb	χ (mrad)	α_2 (mrad)	Θ^2_{rms}	α_{cut} (mrad)	$\Theta^2_{rms,cut}$
1.5	13.7	$2.11 \cdot 10^{-3}$	75.6	$1.09 \cdot 10^{-14}$	4.0	$9.0 \cdot 10^{-15}$
9.0	20.6	$3.52 \cdot 10^{-4}$	12.6	$2.64 \cdot 10^{-16}$	4.0	$2.5 \cdot 10^{-16}$
15.0	22.6	$3.52 \cdot 10^{-4}$	7.56	$9.66 \cdot 10^{-17}$	4.0	$9.6 \cdot 10^{-17}$

rather small, see Table 1. This is due to fact that α_2 enters only logarithmically in Eq. (13). The upper limit $\alpha_{cut} = \Theta_{cut}$ is much more important in the calculation of the beam losses due to single Coulomb scattering as will be shown in Sec. 5.. The resulting values of Θ^2_{rms} and $\Theta^2_{rms,cut}$ are plotted in Fig. 2 as a function of the beam momentum.

2.3 Transverse heating rate due to the beam-target interaction

The transverse heating rate due to the beam-target interaction is given by

$$\frac{1}{\tau_{tr,t}} = \frac{1}{\tau_{x,y,t}} = \frac{\beta_{x,y} \Theta^2_{rms,cut} f}{2 \epsilon_{x,y}}. \tag{18}$$

It is inversely proportional to the momentary transverse emittance $\epsilon_{x,y}$ of the beam. The subscript tr refers to x and y, respectively. In Fig. 3 the resulting values are plotted as a function of the beam momentum p assuming $\Theta_{cut} = 4.0$ mrad and various equilibrium values ϵ_{eq}. The standard mode of operation with a pellet target requires equilibrium emittances of about 1 mm mrad in order to provide a sufficient overlap between beam and target. The corresponding transverse heating rate for 1 mm mrad is very small, see Fig. 3. As a consequennce, the necessary cooling rate for an equilibrium emittance of 1 mm mrad is also very small. We discuss this interrelation in greater detail in Subsec. 7.1.

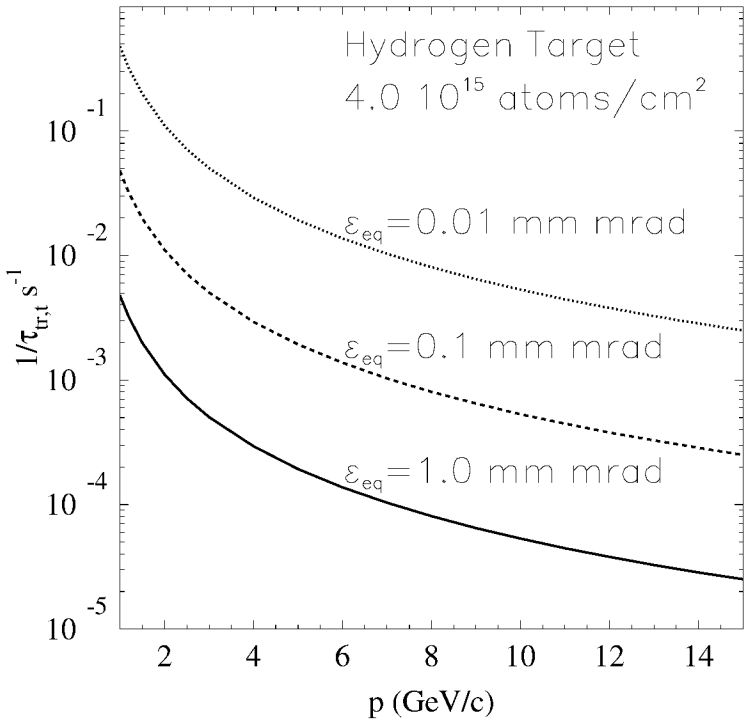

Fig. 3: Transverse heating rate $1/\tau_{tr,t} = 1/\tau_{x,t} = 1/\tau_{y,t}$ due to beam-target interaction vs. p assuming $\Theta^2_{rms,cut}$ as in Fig. 2, $\beta_{x,y} = 1$ m and three equilibrium emittances. $\epsilon_{eq} = 1$ mm mrad refers to the standard mode of operation.

3. Longitudinal Emittance Growth

The formalism to describe longitudinal emittance growth due to beam-target effects is very similar to that of transverse emittance growth. The longitudinal emittance growth depends on the energy straggling of the beam-target interaction. The energy loss of the beam during a target traversal is a consequence of the collisions with the target electrons. This is a statistical process with large fluctuations yielding an energy loss distribution with long tails at HESR energies. Assuming that the mean energy loss is automatically compensated by the synchrotron acceleration and/or the cooling system the longitudinal emittance growth of a bunched beam may be written [8]

$$\Delta\epsilon_l = \frac{1}{2}\beta_l \delta^2_{rms}. \tag{19}$$

Here, $\Delta\epsilon_l$ denotes the longitudinal emittance growth per target traversal, β_l the longitudinal betafunction and δ^2_{rms} the the mean square relative momentum deviation[2] of the beam-target interaction. For a bunched beam $\beta_l = h|\eta|/Q_s$ where h is the harmonic number, η the frequency slip factor and Q_s the number of synchrotron oscillations per turn. Without cooling the rate of longitudinal emittance growth is given by

$$\frac{\mathrm{d}\epsilon_l}{\mathrm{d}t} = \frac{1}{2}\beta_l \delta^2_{rms} f, \tag{20}$$

The corresponding growth of the mean square relative momentum deviation δ^2 of the beam can be obtained by dividing both sides by β_l. This yields

$$\frac{\mathrm{d}\delta^2}{\mathrm{d}t} = \frac{1}{2}\delta^2_{rms} f. \tag{21}$$

[2]Here and in the following text the symbol δ denotes a relative momentum deviation of the beam, $\delta = \Delta p/p$

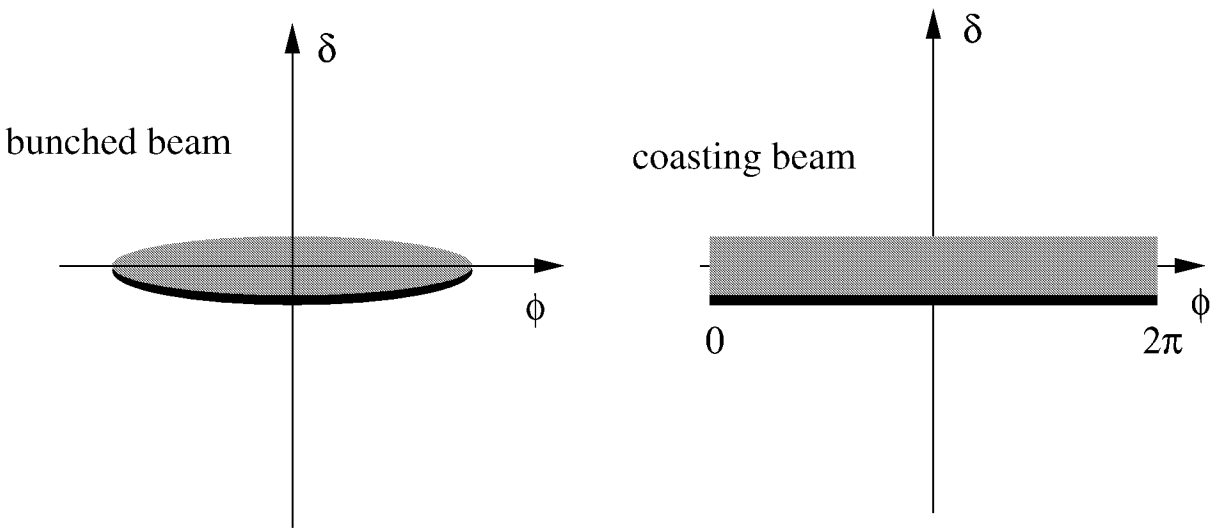

Fig. 4: Longitudinal emittance growth (dark band) per target traversal. Left: bunched beam. Right: coasting beam.

In the case of a coasting beam the factor 1/2 has to be omitted and the mean square relative momentum deviation δ^2 of the beam increases as

$$\frac{\mathrm{d}\delta^2}{\mathrm{d}t} = \delta_{rms}^2 \, f. \tag{22}$$

A pictorial representation of the longitudinal emittance growth per target traversal is shown in Fig. 4. The phase ellipse represents the beam density distribution corresponding to one standard deviation in ϕ and δ. Here, ϕ is the phase lag and δ the relative momentum deviation with respect to the reference particle. The left picture shows the situation for a bunched beam, the right for a coasting beam.

3.1 Energy loss straggling and determination of δ_{rms}^2

In the following we will use the symbol ϵ for the loss of kinetic energy in the target.

Much theoretical effort has been spent to predict energy loss distributions. Depending on the target thickness one can differentiate between the single- plural- and multiple-scattering distributions, the Landau distribution [14], the Vavilov-distribution [15] and the Gaussian distribution. The effective target thickness of the internal target in the HESR ring is $4 \cdot 10^{15}$ hydrogen atoms/cm^2. This value is very small and we are in the regime of single-scattering distributions. Thus, the energy loss distribution resulting from a single target traversal can be calculated using the elementary differential cross section $\mathrm{d}\sigma/\mathrm{d}\epsilon$. The same holds true if one takes the granularity of the pellet target into account where only a small part of the beam sees a pellet with an effective thickness of about $4 \cdot 10^{19}$ atoms/cm^2. If one is interested to see the evolution of the energy loss distribution as a function of time one can for instance start with an elementary single scattering distribution per target traversal. The nth distribution after n turns can be calculated by folding numerically the (n-1)th distribution with the elementary single scattering distribution. This method has been applied for instance in [16].

However, in the following we are only interested in the evolution of the rms width of the energy loss distribution. Fortunately, this quantity can be calculated without a detailed kwowledge of the multiple scattering distributions. The corresponding mean-square energy deviation results from the accumulated contributions of single target traversals. Thus, for any distribution the mean-square energy deviation is just the mean-square value of the elementary *single* scattering distribution per target traversal multiplied by the number of turns.

In order to calculate the energy loss straggling one needs the differential cross section with respect

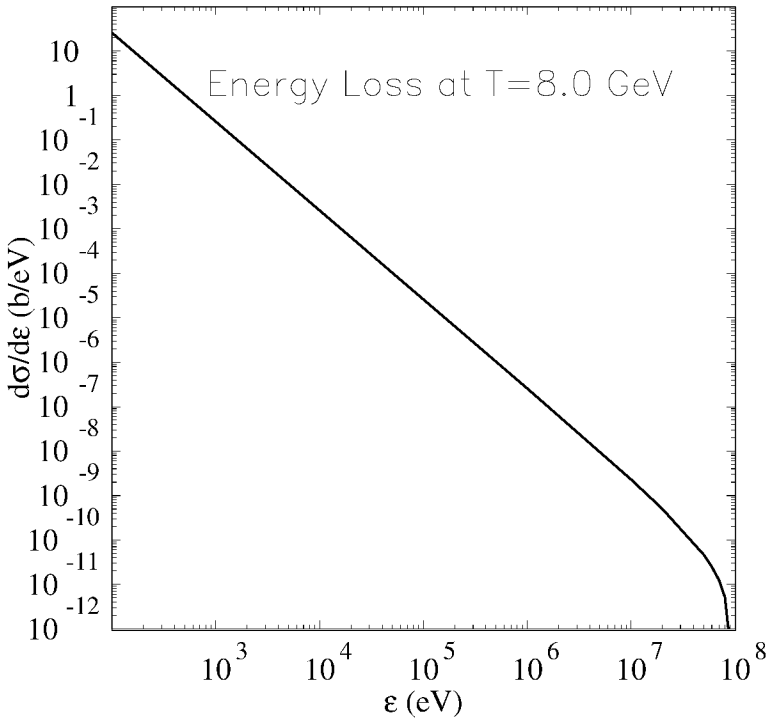

Fig. 5: Differential cross section $\mathrm{d}\sigma/\mathrm{d}\epsilon$ vs. energy loss ϵ.

to the energy loss. Neglecting the very small energy losses due to atomic excitations in the evaluation of the energy straggling and taking only the ionization processes into account the differential cross section $\mathrm{d}\sigma/\mathrm{d}\epsilon$ may be written

$$\begin{aligned} \frac{\mathrm{d}\sigma}{\mathrm{d}\epsilon} &= 2.55 \cdot 10^5 \text{ eV barn } \frac{1}{\beta^2}\left(\frac{1}{\epsilon^2} - \beta^2 \frac{1}{\epsilon \epsilon_{max}}\right) \quad \text{for } \epsilon_i \leq \epsilon \leq \epsilon_{max}, \\ \frac{\mathrm{d}\sigma}{\mathrm{d}\epsilon} &= 0 \quad \text{for } \epsilon < \epsilon_i \text{ and } \epsilon_{max} < \epsilon. \end{aligned} \tag{23}$$

Here, ϵ_i is the ionization energy (for hydrogen $\epsilon_i = 13.6$ eV) and ϵ_{max} is the maximum energy loss which occurs in a head-on collision with a target electron. Outside of the interval $\epsilon_i \leq \epsilon \leq \epsilon_{max}$ $\mathrm{d}\sigma/\mathrm{d}\epsilon = 0$. As an example, Fig. 5 shows the differential cross section $\mathrm{d}\sigma/\mathrm{d}\epsilon$ as a function of the energy loss ϵ for antiprotons with a kinetic energy of 8.0 GeV. The unit of $\mathrm{d}\sigma/\mathrm{d}\epsilon$ is barn/eV=b/eV.

The energy loss straggling can be evaluated by calculating the second moment of the energy loss distribution,

$$\Delta\epsilon^2_{rms} = N_t z_{eff} \int_0^{\epsilon_{max}} \epsilon^2 \left(\frac{\mathrm{d}\sigma}{\mathrm{d}\epsilon}\right) \mathrm{d}\epsilon - \bar{\epsilon}^2. \tag{24}$$

Here, $N_t z_{eff}$ denotes the effective number of target atoms/cm^2. Neglecting the very small terms depending on ϵ_i and $\bar{\epsilon}$ one gets

$$\Delta\epsilon^2_{rms} = \xi \epsilon_{max}\left(1 - \frac{\beta^2}{2}\right) \tag{25}$$

where ξ is a measure of the effective areal target density ρz_{eff},

$$\xi = 0.1535 \frac{\mathrm{MeVcm}^2}{\mathrm{g}} \frac{Z_1^2}{\beta^2} \frac{Z_2}{A_2} \rho z_{eff}. \tag{26}$$

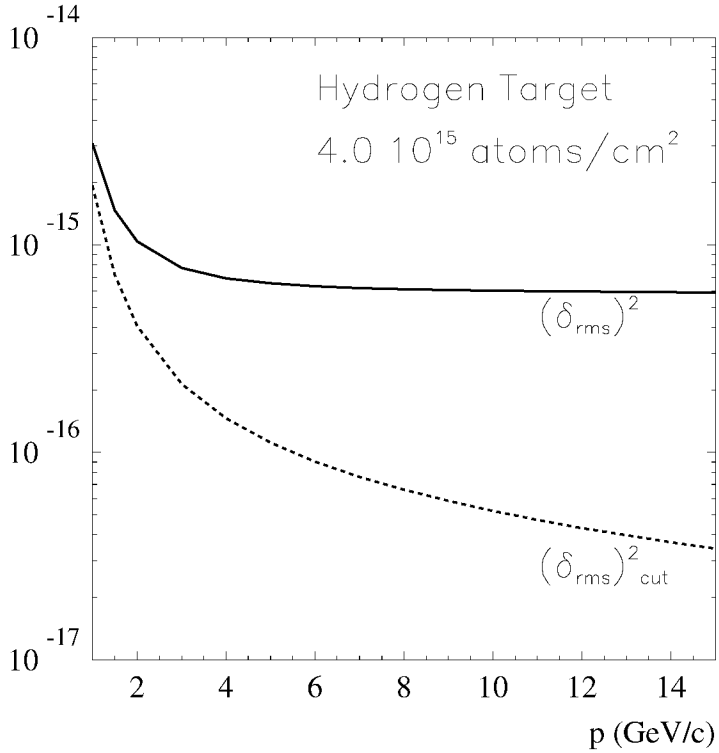

Fig. 6: Mean square relative momentum deviation δ^2_{rms} and $\delta^2_{rms,cut}$ with $\delta_{cut} = 1 \cdot 10^{-3}$ vs. beam momentum p.

The maximum energy loss can be calculated using the formula

$$\epsilon_{max} = \frac{2m_e c^2 \beta^2 \gamma^2}{1 + 2\gamma\frac{m_e}{M} + \frac{m_e^2}{M^2}}. \tag{27}$$

Here, β is the velocity and γ is the Lorentz factor of the beam, m_e the electron mass and M the projectile mass. The corresponding maximum momentum deviation reads

$$\delta_{max} = \frac{\gamma}{\gamma + 1}\frac{\epsilon_{max}}{T}. \tag{28}$$

where T is kinetic beam energy. The resulting equation for δ^2_{rms} reads

$$\delta^2_{rms} = \left(\frac{\gamma}{\gamma + 1}\right)^2 \frac{\Delta\epsilon^2_{rms}}{T^2}. \tag{29}$$

3.2 Restricted energy loss straggling

However, inspecting the resulting values of ϵ_{max} and δ_{max}, it turns out that *the maximum energy loss is too large* in the HESR momentum range from 1.5 – 15 GeV/c. For instance at p=8.9 GeV/c and 15.0 GeV/c $\epsilon_{max} = 90.78$ MeV and 257.7 MeV, respectively. The corresponding relative momentum deviation of $\delta_{max} = 0.0103$ and 0.0174 is outside of the momentum acceptance of the HESR ring. The actual momentum acceptance of the HESR ring corresponds to a relative momentum deviation of about $\pm 1.3 \cdot 10^{-3}$. Thus, the energy loss has to be restricted.

In the following we assume a momentum acceptance of $\delta_{cut} = 1 \cdot 10^{-3}$ which can be adjusted with the aid of beam scrapers in a region of nonzero dispersion. The corresponding value of ϵ_{cut} reads

$$\epsilon_{cut} = \delta_{cut}\frac{\gamma + 1}{\gamma}T. \tag{30}$$

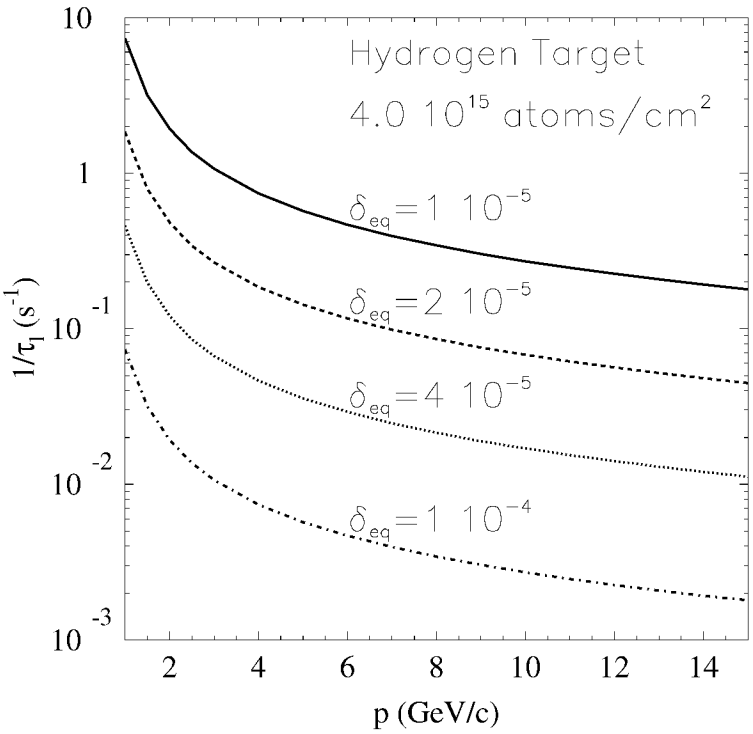

Fig. 7: Restricted energy loss straggling: Longitudinal heating rate $1/\tau_{l,t}$ due to beam-target interaction vs. p assuming $\delta_{cut} = 1 \cdot 10^{-3}$ and four different equilibrium values δ_{eq}. The assumed relative momentum acceptance $\delta_{cut} = 1 \cdot 10^{-3}$ refers to the standard mode of operation.

Taking the restricted energy loss ϵ_{cut} the mean square energy deviation reads

$$\Delta\epsilon^2_{rms} = \xi\epsilon_{cut}\left(1 - \frac{\beta^2}{2}\right). \tag{31}$$

The resulting δ^2_{rms} can be calculated using Eq. (29).

For a hydrogen target with $4 \cdot 10^{15}$ atoms/cm^2 and $\delta_{cut} = 0.001$ we obtain $\epsilon_{cut} = 8.84$ MeV and $\delta^2_{rms,cut} = 5.84 \cdot 10^{-17}$ at $T = 8.0$ GeV which has to be compared with $\delta^2_{rms} = 6.08 \cdot 10^{-16}$ if the energy loss is not restricted. In Fig. 6 the resulting mean square relative momentum deviation $\delta^2_{rms,cut}$ is plotted as a function of the beam momentum for a hydrogen target with an effective target thickness of $4 \cdot 10^{15}$ atoms/cm^2. A substantial restriction of the energy loss has the great advantage that the mean square momentum deviation δ^2_{rms} is an order of magnitude smaller. As a consequence, the necessary cooling rate can be *an order of magnitude smaller* (see Subsec. 7.2). In Sec. 5. we show that the resulting beam losses are still tolerable.

3.3 Longitudinal heating rate due to the beam-target interaction

For a coasting beam, the longitudinal heating rate due to the beam-target interaction is given by

$$\frac{1}{\tau_{l,t}} = \frac{\delta^2_{rms}}{\delta^2} f. \tag{32}$$

It depends on the momentary mean square momentum spread δ^2 of the beam. In Fig. 7 the resulting values are plotted as a function of the beam momentum p assuming $\delta_{cut} = 1 \cdot 10^{-3}$ and various equilibrium

values δ_{eq}. Since the beam-target interaction is the dominating longitudinal heating process the curves of Fig. 7 indicate the cooling rates which are necessary to reach the corresponding equilibrium values δ_{eq}. We discuss this interrelation in greater detail in Subsec. 7.2.

4. Intrabeam Scattering

Besides the beam-target effects intrabeam scattering (IBS) is the most important cause of beam heating. Here, we discuss IBS in order to compare it with the beam-target effects. The beam losses due to IBS will be discussed in Sec. 5..

The IBS is due to the Coulomb interaction between the beam particles. It should be mentioned that Piwinski's work [17] is the origin of all IBS models. The plasma model of Sørensen [18] and the models of Bjorken-Mtingwa [19] and Fedotov [20] provide an analytical description of the transverse and longitudinal emittance growth by the intrabeam scattering. The resulting heating rates are in fair agreement with those calculated numerically with the program BETACOOL using the formalism of Martini [21].

4.1 Longitudinal heating rate due to IBS

We assume an internal beam where the longitudinal velocity spread is small compared to the transverse velocity spread, i.e. the longitudinal temperature of the cooled particles is much smaller than the transverse one, $T_l \ll T_{tr}$. In other words, the rms width of the relative momentum deviation is very small, $\delta \leq 1 \cdot 10^{-4}$. The longitudinal heating, i.e. the rate of change of δ^2, is described by

$$\frac{\mathrm{d}\delta^2}{\mathrm{d}t} = N \frac{\sqrt{\pi}}{4} \frac{c r_p^2 L_C}{\beta^3\gamma^3 < \sqrt{\beta_\perp} > C} \frac{1}{\epsilon_\perp^{3/2}}. \tag{33}$$

Here, N is the number of antiprotons in the ring, $r_p = 1.535 \cdot 10^{-18}$ m the classical proton radius, $L_C = 20$ the Coulomb logarithm, $\beta\gamma$ a measure of the beam momentum, $< \sqrt{\beta_\perp} >$ the average of the square root of the betatron amplitudes in the ring, C the ring's circumference and $\epsilon_\perp = \sqrt{\epsilon_x \epsilon_y}$ a measure of the horizontal and vertical rms beam emittances[3], respectively. The corresponding heating rate $1/\tau_{l,ibs}$ is related to the mean square relative momentum deviation. It is defined by the equation

$$\frac{1}{\tau_{l,ibs}} = \frac{1}{\delta^2} \frac{\mathrm{d}\delta^2}{\mathrm{d}t}. \tag{34}$$

Thus, it may be written

$$\frac{1}{\tau_{l,ibs}} = N \frac{\sqrt{\pi}}{4} \frac{c r_p^2 L_C}{\beta^3\gamma^3 < \sqrt{\beta_\perp} > C} \frac{1}{\epsilon_\perp^{3/2}} \frac{1}{\delta^2}. \tag{35}$$

For a given beam momentum the longitudinal heating rate is proportional to the number N of circulating particles and inversely proportional to $\epsilon_\perp^{3/2}$ and δ^2.

As can be seen, the resulting longitudinal heating rates due to IBS are very large for small emittances. But for transverse emittances of about 1 mm mrad and $p > 3$ GeV/c, the longitudinal heating rates due to IBS are much smaller than the heating rates due to the beam-target interaction (see Figs. 7 and 8)

4.2 Transverse heating rate due to IBS

The rate of change of the transverse emittance ϵ_x, is described by

$$\frac{\mathrm{d}\epsilon_x}{\mathrm{d}t} = \delta^2 \left(\left\langle \frac{D_x^2 + \tilde{D}_x^2}{\beta_x^2} \right\rangle - \frac{1}{\gamma^2} \right) \frac{< \beta_x >}{\tau_{l,ibs}}. \tag{36}$$

[3] We repeat that our definition of $\epsilon_{x,y}$ is such that the emittance $E_{x,y}$ is given by $E_{x,y} = \pi\epsilon_{x,y}$. It differs from the definition of Sørensen [18] where $E_{x,y} = \epsilon_{x,y}$

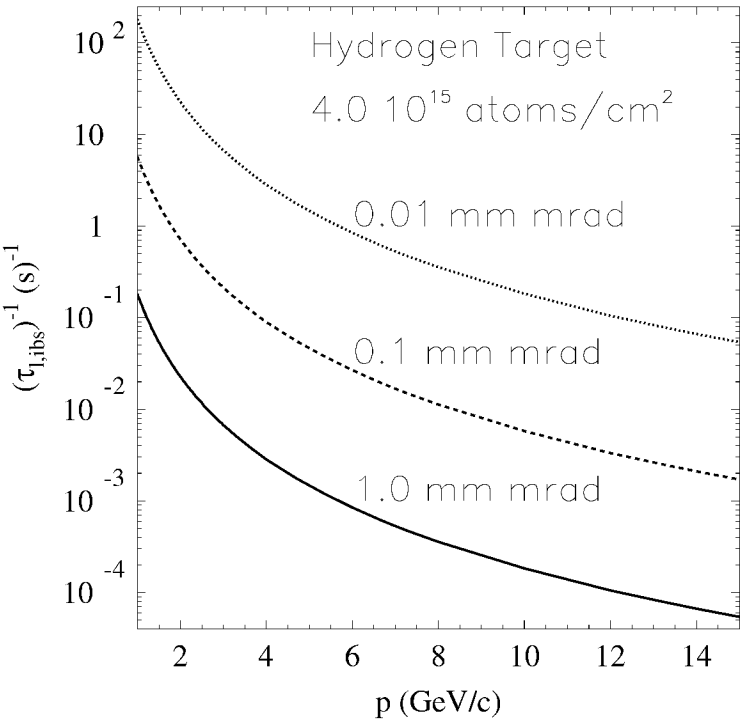

Fig. 8: IBS: Longitudinal heating rates $1/\tau_{l,ibs}$ for $\delta = 1 \cdot 10^{-5}$ and three different transverse equilibrium emittances vs. beam momentum p. $\epsilon_{eq} = 1$ mm mrad refers to the standard mode of operation.

Here, $\tilde{D}_x = D_x\alpha_x + D'_x\beta_x$, D_x and D'_x are the dispersion function and it's derivative, α_x and β_x are the horizontal Twiss parameters and $< (D_x^2 + \tilde{D}_x^2)/\beta_x^2 >$ and $< \beta_x >$ are averages over the ring's circumference. Eq. (36) can be extracted from the theory of Bjorken-Mtwinga [19]. The corresponding heating rate reads

$$\frac{1}{\tau_{x,ibs}} = \frac{\delta^2}{\epsilon_x}\left(\left\langle \frac{D_x^2 + \tilde{D}_x^2}{\beta_x^2} \right\rangle - \frac{1}{\gamma^2}\right)\frac{< \beta_x >}{\tau_{l,ibs}}. \tag{37}$$

For a given beam momentum the transverse heating rate $1/\tau_{x,ibs}$ is proportional to the number N of circulating particles and inversely proportional to $\epsilon_x\epsilon_\perp^{3/2}$. In Fig. 9, the transverse heating rates are shown as a function of the beam momentum p for three different transverse emittances, 1.0, 0.1 and 0.01 mm mrad. The curves have been calculated assuming equal emittances in x- and y-direction, i.e. $\epsilon_x = \epsilon_y = \epsilon_\perp$. Comparing the longitudinal and transverse heating rates due to IBS one sees that the transverse heating rate is much smaller than the longitunal. There is no simple analytic formula for the transverse heating rate $1/\tau_{y,ibs}$ of the vertical emittance. But usually, $1/\tau_{y,ibs}$ is very small compared to $1/\tau_{l,ibs}$ and $1/\tau_{x,ibs}$. Depending on the magnitude of ϵ_y and the structure of the lattice it may even happen that $1/\tau_{y,ibs}$ gets negative, i.e. ϵ_y decreases.

It should be mentioned that the transverse emittances ϵ_x and ϵ_y must be adjusted such that the transverse emittances are relatively large, i.e. $\epsilon_x \approx \epsilon_y \approx 1$ mm mrad, in order to guarantee a good overlap between beam and pellet target. As a consequence, the transverse heating rates due to IBS are much smaller than the heating rates due to the beam-target interaction (compare Fig. 3 with Fig. 9)

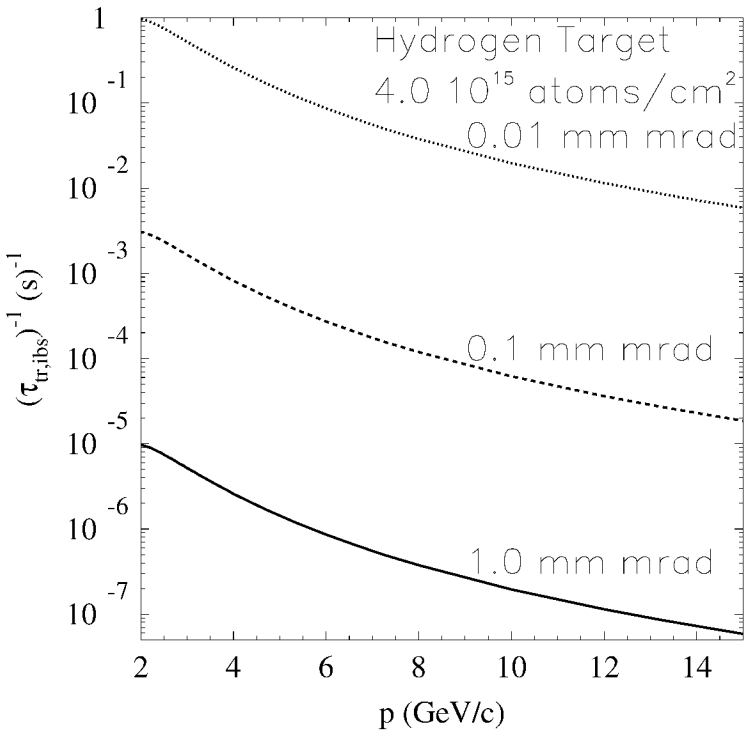

Fig. 9: IBS: Transverse heating rates $1/\tau_{tr,ibs} = 1/\tau_{x,ibs}$ for $\delta = 1 \cdot 10^{-5}$ and three different transverse equilibrium emittances vs. beam momentum p. $\epsilon_{eq} = 1$ mm mrad refers to the standard mode of operation.

5. Beam Losses

How many particles are lost? In the following we discuss various processes leading to particle losses in the ring. The most important losses are due to the hadronic interaction and the single Coulomb scattering between beam and target. In addition one has to consider the losses by setting an upper limit $\delta_{cut} = 1 \cdot 10^{-3}$ for the relative momentum acceptance, i.e. by restricting the energy loss. Another important loss rate related to δ_{cut} is caused by the socalled Touschek effect.

5.1 Losses due to the hadronic beam-target interaction

The total hadronic cross section σ_{tot} for the $\bar{\text{p}}$p interaction depends on the beam momentum. Therefore, the data were fitted in the momentum range 1–15 GeV/c using the following ansatz suggested by analytic S-matrix and Regge theory,

$$\sigma_{tot} = a_1 + a_2 \left(\frac{s}{s_1} \right)^{a_3}. \tag{38}$$

Here, s is the Mandelstam variable of the $\bar{p}p$ system, a_1, a_2 and a_3 are fit parameters and $s_1 = 1$ GeV^2 is a constant. Using the data set of the particle data group [22, 23] we deduce in a nonlinear least-square fit the following parameters

$$\begin{aligned} a_1 &= (48.1 \pm 0.6) \text{ mbarn}, \quad a_2 = (654 \pm 23) \text{ mbarn}, \\ a_3 &= (-1.547 \pm 0.027), \quad \chi^2/ndf = 1.05. \end{aligned} \tag{39}$$

The fit curve with the data is shown in Fig. 10. The loss rate due to the total hadronic cross section is calculated using

$$\frac{1}{\tau_{loss,h}} = N_t z_{eff} \sigma_{tot} f. \tag{40}$$

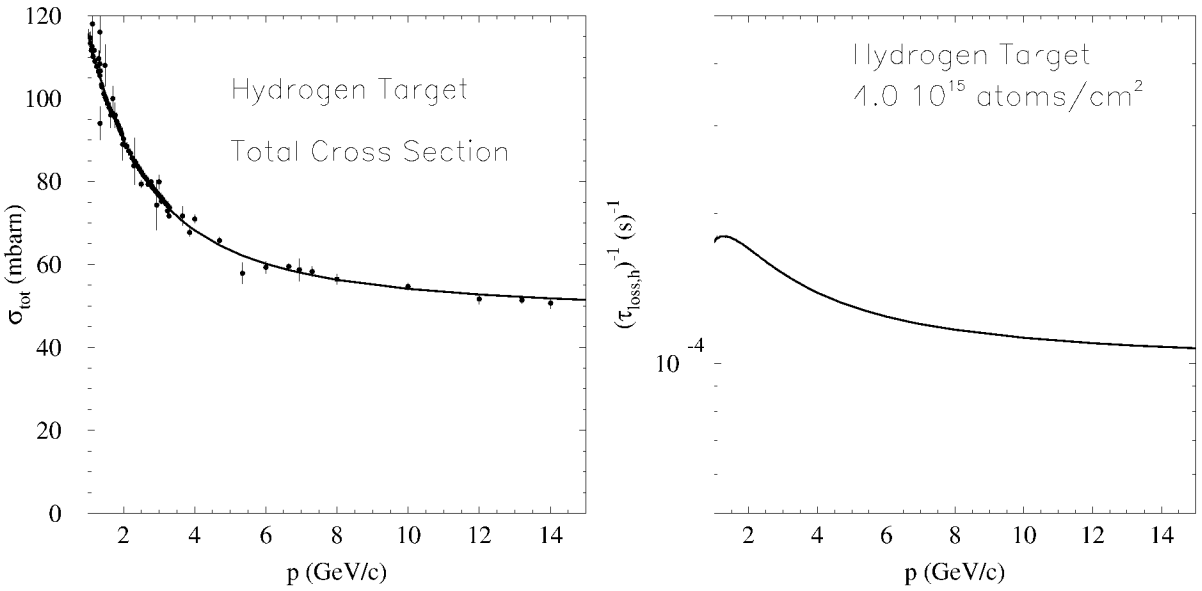

Fig. 10: $\bar{p}+p \rightarrow \bar{p}+p$. Left: Total hadronic cross section σ_{tot} vs. beam momentum p. Solid line: fit curve according Eq. (38). Right: Relative beam loss rate $1/\tau_{loss,h}$ due to the total hadronic cross section σ_{tot} vs. beam momentum p.

The resulting loss rate is shown in Fig. 10 on the right side.

5.2 Single Coulomb scattering losses

Particles which are scattered out of the transverse acceptance are lost. The integrated cross section σ_c for single Coulomb scattering reads

$$\sigma_c = 2\pi \int_{\Theta_{cut}}^{\pi} \frac{\mathrm{d}\sigma_c}{\mathrm{d}\Omega} \sin\Theta \mathrm{d}\Theta = 4\pi \frac{Z_1^2 Z_2^2 r_p^2}{\beta^4 \gamma^2 \Theta_{cut}^2}. \tag{41}$$

Here, Θ_{cut} is the acceptance angle, Z_1 and Z_2 are charge numbers of target and projectile and $r_p = 1.535 \cdot 10^{-18}$ m the classical proton radius. The acceptance angle Θ_{cut} depends on the acceptances $\epsilon_{acc,x}$ and $\epsilon_{acc,y}$ and the betafunctions β_x and β_y at the target position. In the following evaluation we assume common values for the acceptances and the betafunctions, that means $\epsilon_{acc,x} = \epsilon_{acc,y} = \epsilon_{acc}$, $\beta_x = \beta_y = \beta_\perp$. Thus, Θ_{cut} is given by

$$\Theta_{cut} = \sqrt{\frac{\epsilon_{acc}}{\beta_\perp}}. \tag{42}$$

The acceptance ϵ_{acc} depends on the apertures of the ring, the adjustment of beam scrapers and in the case of electron cooling on the overlap between the antiproton beam and the electron beam. The loss rate for single Coulomb scattering is given by

$$\frac{1}{\tau_{loss,c}} = N_t z_{eff} \sigma_c f. \tag{43}$$

Fig. 11 shows the integrated Coulomb cross section and the resulting relative beam loss rate $1/\tau_{loss,c}$ as a function of beam momentum p for $N_t z_{eff} = 4 \cdot 10^{15}$ atoms/cm^2 assuming various acceptance angles Θ_{cut}. The value $\Theta_{cut} = 4$ mrad refers to the standard mode of operation.

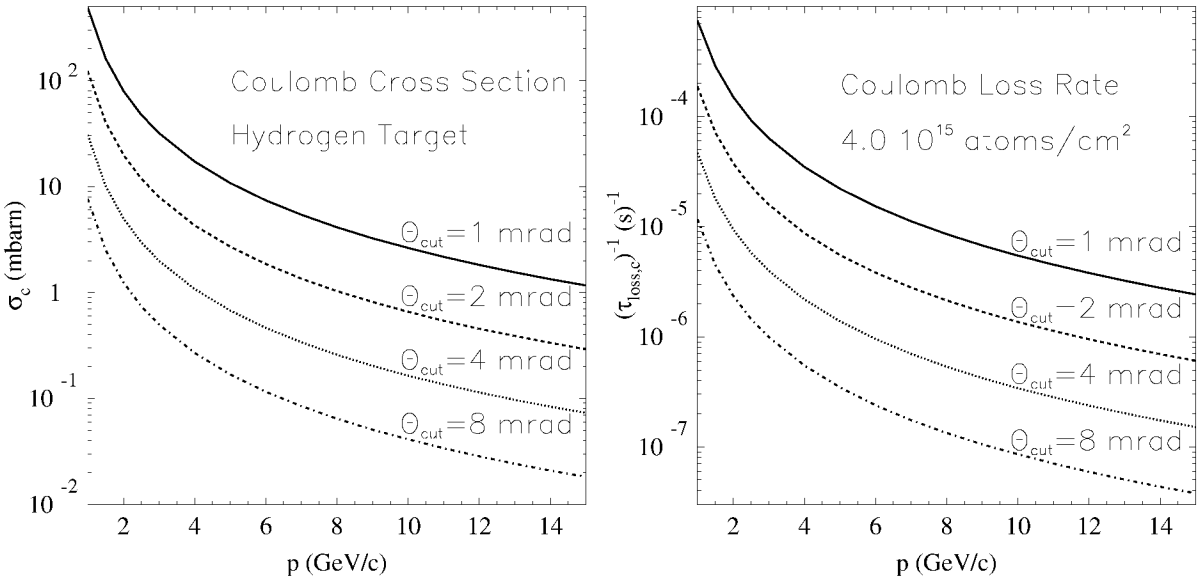

Fig. 11: Left: Integrated Coulomb cross section σ_c vs. beam momentum p. The figure shows σ_c for various acceptance angles Θ_{cut}. Right: Relative beam loss rate $1/\tau_{loss,c}$ due to single Coulomb scattering vs. beam momentum p. The figure shows $1/\tau_{loss,c}$ for various acceptance angles Θ_{cut}. The value $\Theta_{cut} = 4$ mrad refers to the standard mode of operation.

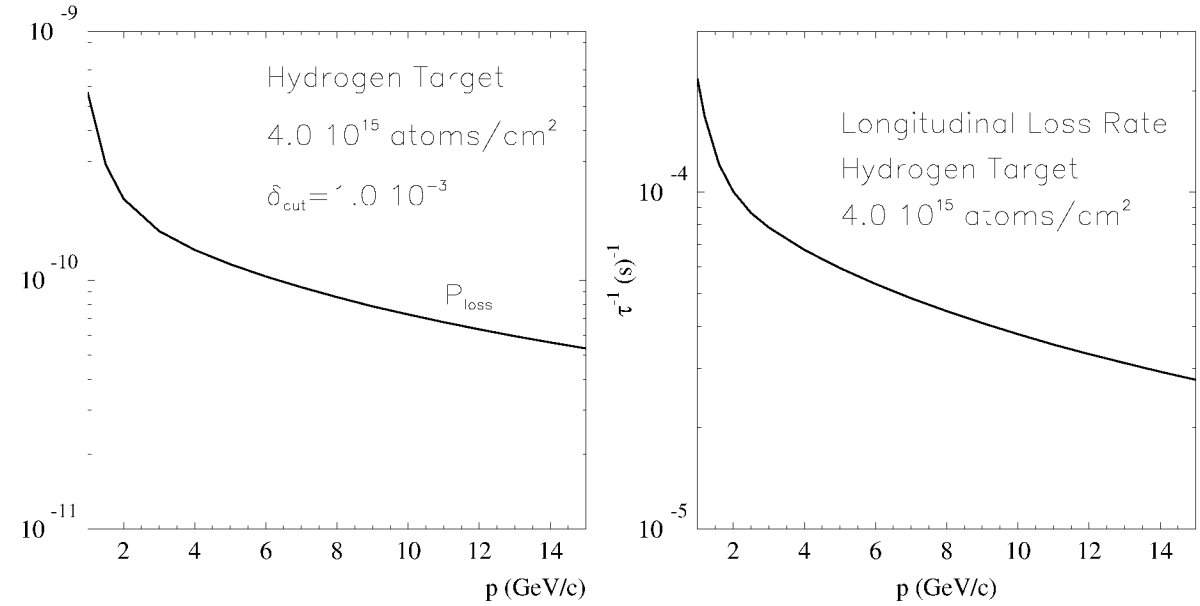

Fig. 12: Beam losses due to restricted energy loss. Left: Loss probability per turn for $\delta_{cut} = 1 \cdot 10^{-3}$. Right: Corresponding longitudinal loss rate $(1/\tau_{loss})_{long}$ vs. beam momentum p.

5.3 Losses due to restricted energy loss

Important particle losses are due to restricting the energy loss by the finite momentum acceptance of the HESR ring. In Sect. 3.2 we considered as a reasonable upper limit $\delta_{cut} = 1 \cdot 10^{-3}$. The corresponding loss probability per turn, P_{loss}, can be calculated by integrating the differential cross section $\mathrm{d}\sigma/\mathrm{d}\epsilon$ from

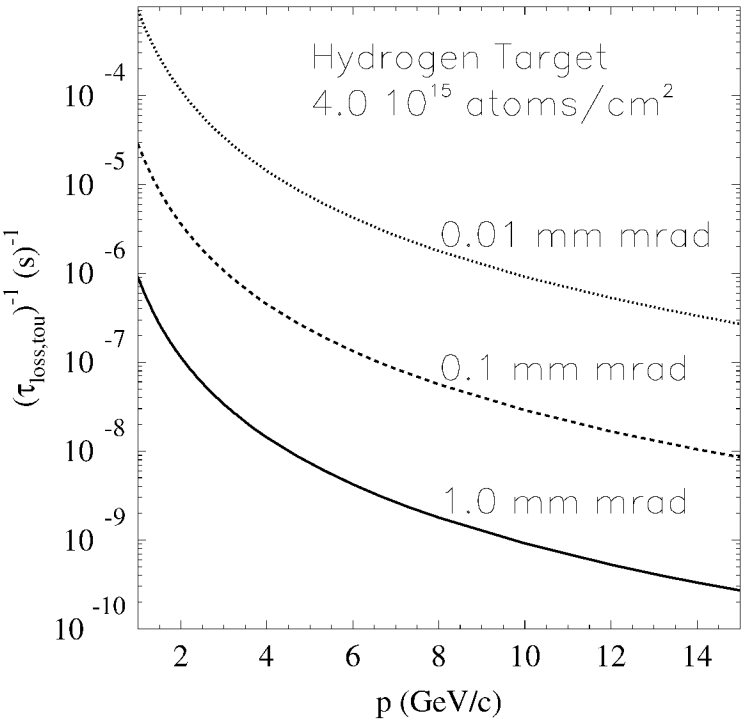

Fig. 13: Beam loss rate $1/\tau_{loss,tou}$ due to the Touschek effect vs. beam momentum p assuming $\delta_{cut} = 1 \cdot 10^{-3}$ and three different transverse equilibrium emittances. $\epsilon_{eq} = 1$ mm mrad refers to the standard mode of operation.

ϵ_{cut} to ϵ_{max},

$$\begin{aligned} P_{loss} &= Nx \int_{\epsilon_{cut}}^{\epsilon_{max}} \frac{\mathrm{d}\sigma}{\mathrm{d}\epsilon} \mathrm{d}\epsilon \\ &= \xi \int_{\epsilon_{cut}}^{\epsilon_{max}} \left(\frac{1}{\epsilon^2} - \beta^2 \frac{1}{\epsilon\, \epsilon_{max}} \right) \mathrm{d}\epsilon \\ &= \xi \left(\frac{1}{\epsilon_{cut}} - \frac{1}{\epsilon_{max}} - \frac{\beta^2}{\epsilon_{max}} \ln \frac{\epsilon_{max}}{\epsilon_{cut}} \right) \end{aligned} \tag{44}$$

The corresponding longitudinal loss rate can be written

$$\frac{1}{\tau_{loss,l}} = P_{loss}\, f. \tag{45}$$

For a hydrogen target with $4 \cdot 10^{15}$ atoms/cm^2, beam momentum $p = 8.889$ GeV/c ($T = 8.0$ GeV) and $\delta_{cut} = 1{\cdot}10^{-3}$ we get $P_{loss} = 7.9{\cdot}10^{-11}$ per target traversal and $1/\tau_{loss,l} = 4.1{\cdot}10^{-5}/\mathrm{s} = 14.8{\cdot}10^{-2}/\mathrm{h}$. At the highest beam momentum $p = 15$ GeV/c ($T = 14.1$ GeV) we get $P_{loss} = 5.3 \cdot 10^{-11}$ per target traversal and $1/\tau_{loss,l} = 2.78 \cdot 10^{-5}/\mathrm{s} = 10.0 \cdot 10^{-2}/\mathrm{h}$. In Fig. 12 the loss probability per turn and the loss rate are shown as a function of the beam momentum.

5.4 Losses due to the Touschek effect

The Touschek effect is a special case of IBS. It is due to the large angle Coulomb scattering within the beam where two particles with large transverse momenta are scattered from the transverse direction into the longitudinal direction. These particles are lost if their longitudinal momentum deviation is outside of

the momentum acceptance δ_{cut}. The corresponding loss rate $1/\tau_{loss,tou}$ can be evaluated [24, 28] using

$$\frac{1}{\tau_{loss,tou}} = N\,\frac{\sqrt{\pi}}{4}\,\frac{cr_p^2}{\beta^3\gamma^3 < \sqrt{\beta_\perp} > C}\,\frac{1}{\epsilon_\perp^{3/2}}\,\frac{1}{\delta_{cut}^2}. \tag{46}$$

The variables are defined in the context of the longitudinal heating rate due to IBS, see Eq. (35). It is interesting to note that the Touschek loss rate is related to the longitudinal heating rate due to IBS,

$$\frac{1}{\tau_{loss,tou}} = \frac{1}{\tau_{l,ibs}}\,\frac{1}{L_c}\,\frac{\delta^2}{\delta_{cut}^2}. \tag{47}$$

In Fig. 13 the loss rates due to the Touschek effect are plotted as a function of the beam momentum p for three different transverse emittances $\epsilon_\perp$ assuming a momentum acceptance $\delta_{cut} = 1 \cdot 10^{-3}$. For a given beam momentum the loss rate due to Touschek is proportional to the number N of circulating particles and inversely proportional to $\epsilon_\perp^{3/2}$ and $\beta^3\gamma^3$. For transverse emittances of about 1 mm mrad the Touschek losses are negligible compared to the other losses. The losses become dangerously large for very small transverse emittances, e.g. 0.001 mm mrad and less.

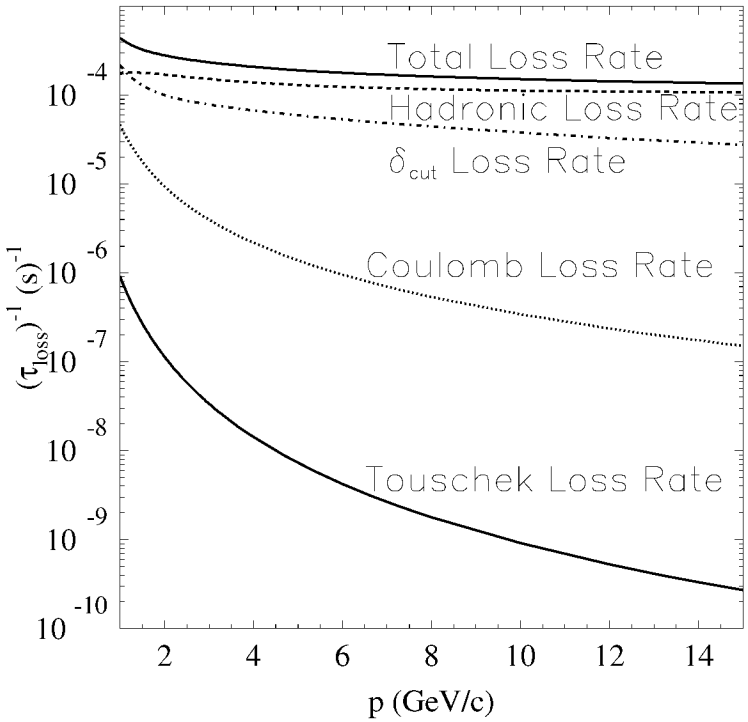

Fig. 14: Total loss rate $1/\tau_{loss}$. The loss rates have been evaluated assuming the standard mode of operation with $\epsilon_{eq} = 1$ mm mrad, $\Theta_{cut} = 4$ mrad and $\delta_{cut} = 1 \cdot 10^{-3}$.

5.5 Total loss rate

The total loss rate is just the sum of the individual loss rates,

$$\frac{1}{\tau_{loss}} = \frac{1}{\tau_{loss,h}} + \frac{1}{\tau_{loss,l}} + \frac{1}{\tau_{loss,c}} + \frac{1}{\tau_{loss,tou}}. \tag{48}$$

Here, $1\tau_{loss,h}$ denotes the loss rate due to the total hadronic cross section, $1/\tau_{loss,l}$ the loss rate due to the finite relative momentum acceptance δ_{cut}, $1/\tau_{loss,c}$ the loss rate due to the large angle single Coulomb scattering and $1/\tau_{loss,tou}$ the loss rate due to the Touschek effect, In Fig. 14 the individual and total loss rates are shown as a function of the beam momentum p. All loss rates have been evaluated assuming the standard mode of operation with $\epsilon_{eq} = 1$ mm mrad, $\Theta_{cut} = 4$ mrad and $\delta_{cut} = 1 \cdot 10^{-3}$.

It should be noted that the loss rates would be drastically higher if one would assume very small equilibrium emittances of about $1 \cdot 10^{-3}$ mm mrad and a maximum scattering angle of only $\Theta_{cut} = 1$ mrad.

6. Average Luminosity

Concerning the average luminosity which can be reached in the HESR we refer to a recent paper by Lehrach et al. [25]. The achievable average luminosity $\bar{L}$ depends on the effective target thickness $N_t z_{eff}$, the revolution frequency f and the average number $\bar{N}$ of antiprotons in the ring averaged over the full cycle time t_{cycle},

$$\bar{L} = \bar{N}\, f\, N_t\, z_{eff}. \tag{49}$$

The quantity $\bar{N}$ which is of great importance for the experiment depends on the production rate $\mathrm{d}N_{prod}/\mathrm{d}t$ of antiprotons and the total loss rate $1/\tau_{loss}$. If it would be possible to inject the produced antiprotons continuously into the HESR ring one could deduce the average number $\bar{N}$ of particles in the ring as the equilibrium between injected and lossed antiprotons. The time dependence of the number of particles in the ring is given by

$$\frac{\mathrm{d}N}{\mathrm{d}t} = -\frac{N}{\tau_{loss}} + \frac{\mathrm{d}N_{prod}}{\mathrm{d}t} \tag{50}$$

The solution of this differential equation yields

$$N(t) = \frac{\mathrm{d}N_{prod}}{\mathrm{d}t}\,\tau_{loss}\left[1 - \exp\left(-\frac{t}{\tau_{loss}}\right)\right]. \tag{51}$$

The above mentioned equilibrium condition $\mathrm{d}N/\mathrm{d}t = 0$ yields

$$N_{eq} = \frac{\mathrm{d}N_{prod}}{\mathrm{d}t}\,\tau_{loss}. \tag{52}$$

These equations show that the upper limit of the average number $\bar{N}$ of particles in the ring is given by the equilibrium value N_{eq} which is reached after several mean lifetimes τ_{loss},

$$\bar{N} = N_{eq} = \frac{\mathrm{d}N_{prod}}{\mathrm{d}t}\,\tau_{loss}. \tag{53}$$

However, the antiprotons can only be injected from time to time. In between, they are accumulated in the RESR ring. Thus, a typical cycle consists of injection of antiprotons from the RESR into the HESR at the injection momentum 3.8 GeV/c, beam preparation, i.e. precooling, acceleration or deceleration to the desired beam momentum and beam cooling to the desired transverse emittance and momentum resolution, data taking by the experiment and preparation of the HESR ring for the next injection. Thus, one can define an overall beam preparation time t_{prep} (typical value 100 – 300 s) and an experimental time t_{exp} (e.g. $t_{exp} = 0.5\tau_{loss}$) which can be used by the experiment. The sum of both define the cycle time t_{cycle},

$$t_{cycle} = t_{prep} + t_{exp}. \tag{54}$$

Under these assumptions, the number of particles which can be injected from time to time into the HESR ring is given by

$$N_{inj} = \frac{\mathrm{d}N_{prod}}{\mathrm{d}t}\,t_{cycle}. \tag{55}$$

The average number of particles which can be used by the eperiment can be deduced using

$$\bar{N} = \frac{N_{inj}}{t_{cycle}} \int_0^{t_{exp}} \exp\left(-\frac{t}{\tau_{loss}}\right) \mathrm{d}t. \tag{56}$$

It should be noted that we average with respect to the full cycle time $t_{cycle} = t_{prep} + t_{exp}$. This yields the following expression for the average number $\bar{N}$ of particles if we assume that the antiprotons are dumped at the end of the cycle,

$$\begin{aligned} \bar{N} &= \frac{N_{inj}}{t_{cycle}} \tau_{loss} \left[1 - \exp\left(-\frac{t_{exp}}{\tau_{loss}}\right)\right] \\ &= \frac{\mathrm{d}N_{prod}}{\mathrm{d}t} \tau_{loss} \left[1 - \exp\left(-\frac{t_{exp}}{\tau_{loss}}\right)\right]. \end{aligned} \tag{57}$$

However, if the residual antiprotons are transferred back to the injection momentum and merged with the newly injected antiprotons without losses, one can again reach the theoretical limit as given by Eq. (53). This statement can be proven by considering the sequence of cycles with respect to the number of particles at the beginning of each data taking period:

$$\begin{aligned} \text{1st cycle} &: N_{inj} \\ \text{2nd cycle} &: N_{inj} \left[1 + \exp\left(-\frac{t_{exp}}{\tau_{loss}}\right)\right] \\ \text{3rd cycle} &: N_{inj} \left[1 + \exp\left(-\frac{t_{exp}}{\tau_{loss}}\right) + \left[\exp\left(-\frac{t_{exp}}{\tau_{loss}}\right)\right]^2\right] \\ n\text{th cycle} &: N_{inj} \sum_{i=1}^{n} \left[\exp\left(-\frac{t_{exp}}{\tau_{loss}}\right)\right]^{i-1} \end{aligned} \tag{58}$$

The limes of this geometric series is given by

$$N_{inj} \left[1 - \exp\left(-\frac{t_{exp}}{\tau_{loss}}\right)\right]^{-1}. \tag{59}$$

Thus, replacing in Eq. (57) N_{inj} by $N_{inj}[1-\exp\left(-t_{exp}/\tau_{loss}\right)]^{-1}$ yields the expression given in Eq. (53). In other words, after several cycles, the average number $\bar{N}$ tends asymptotically towards the upper limit given by the production rate and the time constant τ_{loss},

$$\bar{N} \rightarrow \frac{\mathrm{d}N_{prod}}{\mathrm{d}t} \tau_{loss}. \tag{60}$$

It should be noted that this result has been derived under the assumption that additional beam losses during the beam preparation can be neglected. Taking a particle loss of 10 % in the recycling process into account yields the following modification of Eq. (60),

$$\bar{N} \rightarrow \frac{\mathrm{d}N_{prod}}{\mathrm{d}t} \tau_{loss} \left[1 - \exp\left(-\frac{t_{exp}}{\tau_{loss}}\right)\right] \left[1 - 0.9 \exp\left(-\frac{t_{exp}}{\tau_{loss}}\right)\right]^{-1} \tag{61}$$

Using Eqs. (57) and (61), the achievable upper limits of $\bar{N}$ have been calculated assuming a total loss rate as shown in Fig. 14 and the following production rate

$$\frac{\mathrm{d}N_{prod}}{\mathrm{d}t} = 8 \cdot 10^6 \ \mathrm{s}^{-1}. \tag{62}$$

The resulting average luminosities $\bar{L}$ have been calculated using Eq. (49) and assuming an effective target thickness of $4 \cdot 10^{15}$ atoms/cm^2. Concerning the total length of a cycle it is reasonable to assume

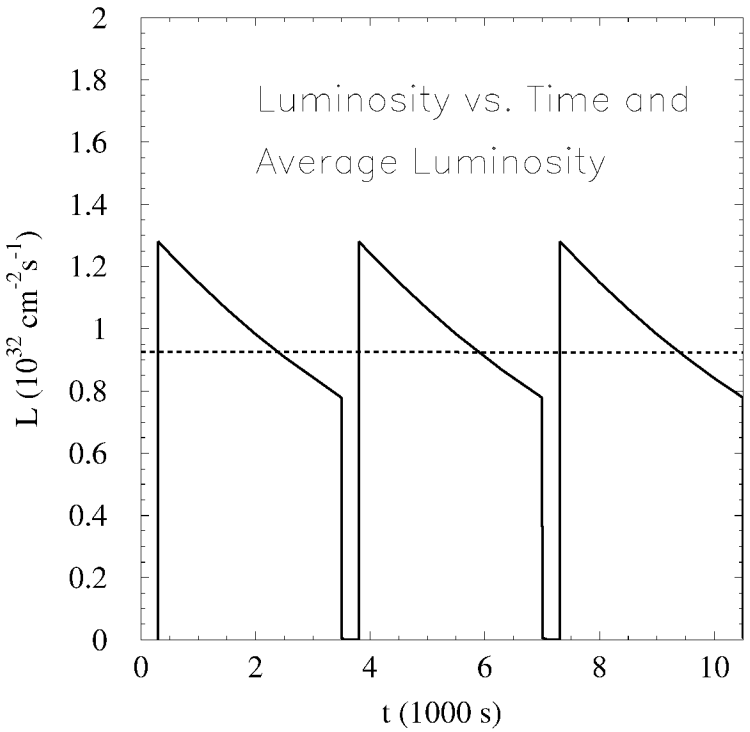

Fig. 15: Luminosity L vs. time t at $p = 9.0$ GeV/c. The figure shows a typical example of the recycling mode of operation with $t_{cycle} = 3500$ s, $t_{prep} = 300$ s and $t_{exp} = 3200$ s. The dashed curve shows the resulting average luminosity $\bar{L}$. The luminosity has been calculated assuming a production rate $\mathrm{d}N_{prod}/\mathrm{d}t = 8 \cdot 10^6$ s^{-1}, an effective target thickness of $4 \cdot 10^{15}$ atoms/cm^2 and a total loss rate of $1.56 \cdot 10^{-4}$ s^{-1}, see Fig. 14. In the recycling process, a particle loss of 10 % has been taken into account. The peak luminosity at the start of each data taking period corresponds to $6 \cdot 10^{10}$ antiprotons in the ring. At the end of each cycle about $3.8 \cdot 10^{-10}$ antiprotons are left for recycling.

$t_{exp} = 0.5\tau_{loss}$ for the recycling mode. Then, the luminosity ratio between stop and start of each data taking period is $1/\sqrt{\mathrm{e}} = 0.61$. That means $t_{cycle} = t_{prep} + 0.5\tau_{loss}$.

Fig. 15 shows a typical plot of the luminosity as a function of time. The beam momentum is 9 GeV/c. We assume the recycling mode of operation with a particle loss of 10 % during the recycling process, see Eq. (61). The characteristic time periods of one cycle are chosen to be $t_{cycle} = 3500$ s, $t_{prep} = 300$ s and $t_{exp} = 3200$ s. The experimental time period t_{exp} corresponds to $0.5\tau_{loss}$. The solid line shows the momentary luminosity as a function of time. The luminosity at the start and stop of each data taking period corresponds to $6 \cdot 10^{10}$ and $3.8 \cdot 10^{10}$ antiprotons in the ring, respectively. The dashed line shows the resulting average luminosity where the average is taken with respect to the full cycle time $t_{cycle} = t_{prep} + t_{exp}$.

In Fig. 16 the maximum average luminosity $\bar{L}$ is shown as a function of the beam momentum p. The solid line represents $\bar{L}$ assuming recycling of the unused antiprotons at the end of each cycle, see Eq. (61). The dashed line represents $\bar{L}$ assuming that the residual antiprotons are dumped at the end of each cycle, see Eq. (57) with $t_{exp} = 0.5\tau_{loss}$. As can be seen, recycling the antiprotons yields maximum average luminosities between $0.37 \cdot 10^{32}$ and $1.05 \cdot 10^{32}$ cm^{-2}s^{-1}. Dumping the antiprotons at the end of each cycle yields maximum average luminosities between $0.17 \cdot 10^{32}$ and $0.48 \cdot 10^{32}$ cm^{-2}s^{-1}.

The maximum average luminosities which can be achieved using the recycling mode are more than a factor of two smaller than the original goal of $2.0 \cdot 10^{32}$ cm^{-2}s^{-1}. This is due to the fact that the antiproton production rate has been reduced in stage 1 from the original value of $2 \cdot 10^7$ s^{-1} to $8 \cdot 10^6$ s^{-1}.

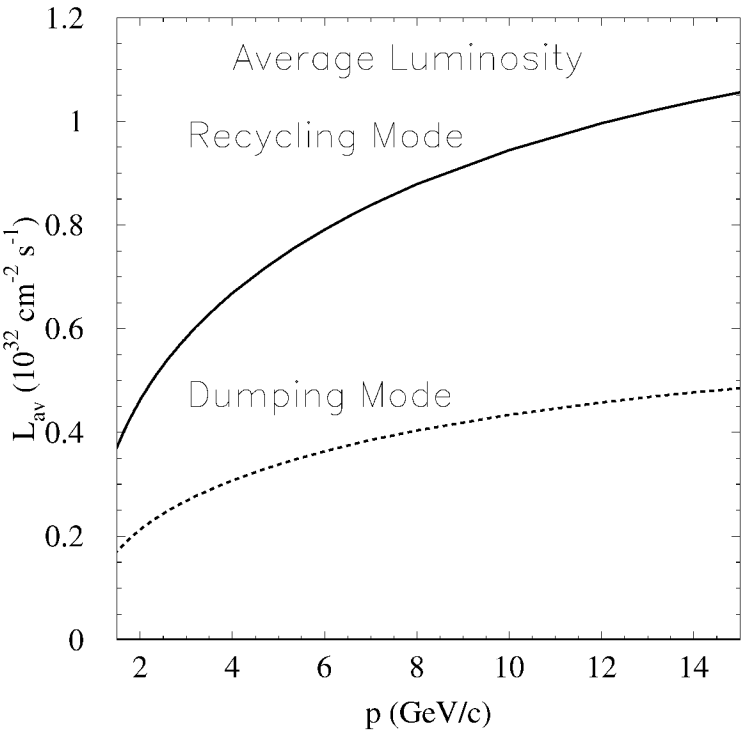

Fig. 16: Maximum average luminosity $L_{av} = \bar{L}$ vs. beam momentum p. Cycle time t_{cycle} is 1834 s at 1.5 GeV/c, 3500 s at 9 GeV/c and 3998 s at 15 GeV/c with $t_{prep} = 300$ s, $t_{exp} = 0.5\tau_{loss}$ and $t_{cycle} = t_{prep} + t_{exp}$. The solid line has been calculated assuming that the residual antiprotons at the end of each cycle are recycled with 90 % efficiency. It represents the upper limit for the average number of antiprotons in the HESR ring as given by Eq. (61) with $\mathrm{d}N_{prod}/\mathrm{d}t = 8 \cdot 10^6$ s^{-1}, an effective target thickness of $4 \cdot 10^{15}$ atoms/cm^2 and a total loss rate as shown in Fig. 14. The corresponding number of antiprotons at the start of data taking varies between $3 \cdot 10^{10}$ at 1.5 GeV/c, $6 \cdot 10^{10}$ at 9 GeV/c and $7 \cdot 10^{10}$ at 15 GeV/c. The dashed line has been calculated assuming that the antiprotons are dumped at the end of each cycle. Here, Eq. (57) has been used with $t_{exp} = 0.5\tau_{loss}$.

The design luminosity of $2.0 \cdot 10^{32}$ cm^{-2}s^{-1} can be achieved in a later stage by upgrading the antiproton production rate.

7. Equilibrium between Beam Cooling and Beam Heating

7.1 Equilibrium transverse emittance and transverse cooling rate

In the following, we omit the subscripts x and y which are used to distinguish between horizontal and vertical direction. Thus, ϵ, β and τ_{tr} represent either ϵ_x, β_x and τ_x or ϵ_y, β_y and τ_y, respectively. The time dependence of the transverse emittances ϵ is described by the differential equation

$$\frac{\mathrm{d}\epsilon}{\mathrm{d}t} = \left(\frac{\mathrm{d}\epsilon}{\mathrm{d}t}\right)_{cooling} + \left(\frac{\mathrm{d}\epsilon}{\mathrm{d}t}\right)_{heating} . \tag{63}$$

The terms describing the cooling and heating processes are negative and positive, respectively. The beam-target interaction and the intra-beam scattering (IBS) are the main sources of beam heating. Other beam heating processes like beam-wall interactions, interactions with the residual gas and positive ions in the ring etc. should also be mentioned. Taking all these processes into account and introducing the

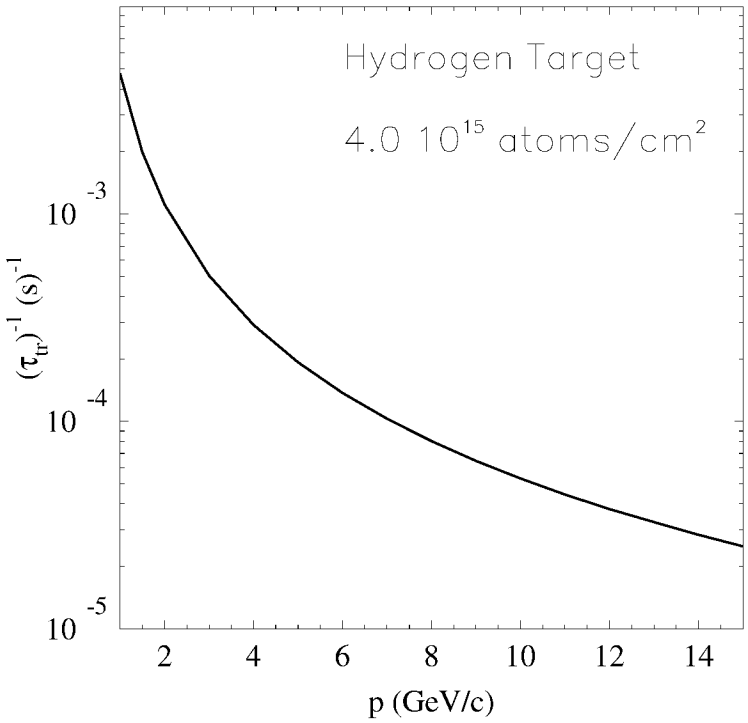

Fig. 17: Transverse cooling rate $1/\tau_{tr}$ for $\epsilon_{eq} = 1$ mm mrad, $\beta = 1$ m, $\theta_{cut} = 4$ mrad and $4 \cdot 10^{15}$ atoms/cm^2 vs. beam momentum. The chosen parameters refer to the standard mode of operation.

cooling rate $1/\tau$ Eq. (63) may be written

$$\frac{\mathrm{d}\epsilon}{\mathrm{d}t} = \overbrace{-\frac{1}{\tau_{tr}}\epsilon}^{cooling} + \overbrace{\frac{1}{2}\beta\Theta_{rms}^2 f + \left(\frac{\mathrm{d}\epsilon}{\mathrm{d}t}\right)_{IBS} + \left(\frac{\mathrm{d}\epsilon}{\mathrm{d}t}\right)_{other}}^{heating}. \tag{64}$$

The equilibrium between cooling and heating is reached if $\mathrm{d}\epsilon/\mathrm{d}t = 0$, yielding the equation for the

Table 2: Transverse cooling rate $1/\tau_{tr}$ for $\epsilon_{eq} = 1$ mm mrad, $\beta = 1$ m, $\theta_{cut} = 4$ mrad and $4 \cdot 10^{15}$ atoms/cm^2

T (GeV)	Θ_{rms}^2	f (MHz)	τ_{tr} (s)	$1/\tau_{tr}$ (s^{-1})
2.0	$2.34 \cdot 10^{-15}$	0.4949	$1.72 \cdot 10^{3}$	$5.80 \cdot 10^{-4}$
4.0	$7.95 \cdot 10^{-16}$	0.5128	$4.91 \cdot 10^{3}$	$2.04 \cdot 10^{-4}$
6.0	$4.12 \cdot 10^{-16}$	0.5175	$9.39 \cdot 10^{3}$	$1.06 \cdot 10^{-4}$
8.0	$2.55 \cdot 10^{-16}$	0.5194	$1.51 \cdot 10^{4}$	$6.61 \cdot 10^{-5}$
10.0	$1.74 \cdot 10^{-16}$	0.5204	$2.21 \cdot 10^{4}$	$4.53 \cdot 10^{-5}$
12.0	$1.27 \cdot 10^{-16}$	0.5209	$3.02 \cdot 10^{4}$	$3.31 \cdot 10^{-5}$
14.0	$9.71 \cdot 10^{-17}$	0.5213	$3.95 \cdot 10^{4}$	$2.53 \cdot 10^{-5}$

equilibrium emittance ϵ_{eq},

$$\epsilon_{eq} = \frac{1}{2}\beta\Theta_{rms}^2 f \tau_{tr} + \left[\left(\frac{\mathrm{d}\epsilon}{\mathrm{d}t}\right)_{IBS} + \left(\frac{\mathrm{d}\epsilon}{\mathrm{d}t}\right)_{other}\right]\tau_{tr}. \tag{65}$$

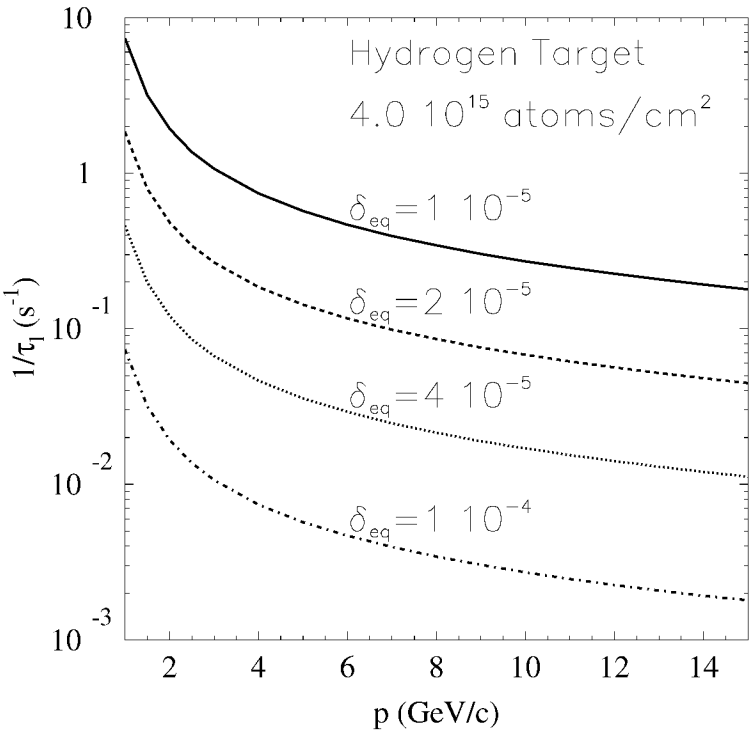

Fig. 18: Longitudinal cooling rates $1/\tau_l$ vs. beam momentum p. The figure shows the cooling rates needed to reach the equilibrium values $\delta_{eq} = 1 \cdot 10^{-5},\ 2 \cdot 10^{-5}, 4 \cdot 10^{-5}$ and $1 \cdot 10^{-4}$. The relative momentum acceptance is $\delta_{cut} = 1 \cdot 10^{-3}$ (standard mode of operation) and the effective target thickness $4 \cdot 10^{15}$ atoms/cm^2.

Now we assume that an equilibrium emittance of about 1 mm mrad should be adjusted in order to get a good overlap with a pellet target. Under this condition the IBS heating rate is negligibly small compared to the beam-target heating effects. The same holds true for all other heating effects. Thus, neglecting the terms $(\mathrm{d}\epsilon/\mathrm{d}t)_{IBS}$ and $(\mathrm{d}\epsilon/\mathrm{d}t)_{other}$ we get the equation

$$\epsilon_{eq} = \frac{1}{2}\beta\Theta_{rms}^2\, f\, \tau_{tr} \tag{66}$$

which allows to deduce the necessary cooling rate

$$\frac{1}{\tau_{tr}} = \frac{1}{\epsilon_{eq}}\frac{1}{2}\beta\Theta_{rms}^2\, f \tag{67}$$

which is equal to the beam-target heating rate, see Eq. (18). In Table 2 and Fig. 17 the resulting values are shown as a function of the beam energy and momentum, respectively, assuming $\beta = 1$ m and $\epsilon_{eq} = 1$ mm mrad.

7.2 Equilibrium momentum spread and longitudinal cooling rate

The time dependence of the mean-square relative momentum spread of the beam, δ^2, is described by the differential equation [26]

$$\frac{\mathrm{d}\delta^2}{\mathrm{d}t} = \left(\frac{\mathrm{d}\delta^2}{\mathrm{d}t}\right)_{cooling} + \left(\frac{\mathrm{d}\delta^2}{\mathrm{d}t}\right)_{heating}. \tag{68}$$

Again, the terms describing the cooling and heating processes are negative and positive, respectively.

The beam-target interaction and the intra-beam scattering (IBS) are the main sources of beam heating. Beam-wall interactions, interactions with the residual gas and positive ions in the ring etc. can also affect the momentum spread. Taking all these processes into account and introducing the cooling rate $1/\tau_l$ and the target heating term for a coasting beam (see Eq. (22)) Eq. (68) may be written

$$\frac{\mathrm{d}\delta^2}{\mathrm{d}t} = \overbrace{-\frac{1}{\tau_l}\,\delta^2}^{cooling} + \overbrace{\delta^2_{rms} f + \left(\frac{\mathrm{d}\delta^2}{\mathrm{d}t}\right)_{IBS} + \left(\frac{\mathrm{d}\delta^2}{\mathrm{d}t}\right)_{other}}^{heating}. \tag{69}$$

The equilibrium between cooling and heating is reached if $\mathrm{d}\delta^2/\mathrm{d}t = 0$, yielding the equation for the

Table 3: Longitudinal cooling rates $1/\tau_l$ for $\delta_{eq} = 1 \cdot 10^{-5}$, $\delta_{cut} = 1 \cdot 10^{-3}$ and $4 \cdot 10^{15}$ atoms/cm^2

T (GeV)	δ^2_{rms}	f (MHz)	τ_l (s)	$1/\tau_l$ (s^{-1})
2.0	$2.38 \cdot 10^{-16}$	0.4949	0.85	1.18
4.0	$1.15 \cdot 10^{-16}$	0.5128	1.69	0.592
6.0	$7.78 \cdot 10^{-17}$	0.5175	2.48	0.403
8.0	$5.91 \cdot 10^{-17}$	0.5194	3.26	0.307
10.0	$4.78 \cdot 10^{-17}$	0.5204	4.02	0.249
12.0	$4.01 \cdot 10^{-17}$	0.5209	4.78	0.209
14.0	$3.46 \cdot 10^{-17}$	0.5213	5.54	0.180

Table 4: Longitudinal cooling rates $1/\tau_l$ for $\delta_{eq} = 4 \cdot 10^{-5}$, $\delta_{cut} = 1 \cdot 10^{-3}$ and $4 \cdot 10^{15}$ atoms/cm^2.

T (GeV)	δ^2_{rms}	f (MHz)	τ_l (s)	$1/\tau_l$ (s^{-1})
2.0	$2.38 \cdot 10^{-16}$	0.4949	13.6	0.0735
4.0	$1.15 \cdot 10^{-16}$	0.5128	27.0	0.0370
6.0	$7.78 \cdot 10^{-17}$	0.5175	39.7	0.0252
8.0	$5.91 \cdot 10^{-17}$	0.5194	52.1	0.0192
10.0	$4.78 \cdot 10^{-17}$	0.5204	64.4	0.0155
12.0	$4.01 \cdot 10^{-17}$	0.5209	76.5	0.0131
14.0	$3.46 \cdot 10^{-17}$	0.5213	88.6	0.0113

equilibrium value δ^2_{eq} of the mean square relative momentum spread,

$$\delta^2_{eq} = \delta^2_{rms} f \tau_l + \left[\left(\frac{\mathrm{d}\delta^2}{\mathrm{d}t}\right)_{IBS} + \left(\frac{\mathrm{d}\delta^2}{\mathrm{d}t}\right)_{other}\right] \tau_l. \tag{70}$$

As in the previous subsection, we assume a transverse equilibrium emittance of about 1 mm mrad in x and y direction in order to get a good overlap with a pellet target. Under this condition the longitudinal IBS heating rate is negligibly small compared to the beam-target heating effects. The same holds true for all other heating effects. Thus, neglecting the terms $(\mathrm{d}\delta^2/\mathrm{d}t)_{IBS}$ and $(\mathrm{d}\delta^2/\mathrm{d}t)_{other}$ we get the equation

$$\delta^2_{eq} = \delta^2_{rms} f \tau_l \tag{71}$$

which allows to deduce the necessary cooling rate

$$\frac{1}{\tau_l} = \frac{\delta^2_{rms}}{\delta^2_{eq}}\, f, \tag{72}$$

which is equal to the beam-target heating rate, see Eq. (32). The mean square values δ^2_{rms} which are due to the energy straggling per target traversal are calculated assuming a restricted momentum loss of $\delta_{cut} = 1 \cdot 10^{-3}$, see Subsec. 3.2. In Tables 3 and 4 the cooling rates are listed for $\delta_{eq} = 1 \cdot 10^{-5}$ and $\delta_{eq} = 4 \cdot 10^{-5}$. In Fig. 18 the longitudinal cooling rates are shown as a function of the beam momentum assuming $\delta_{eq} = 1 \cdot 10^{-5},\ 2 \cdot 10^{-5}, 4 \cdot 10^{-5}$ and $1 \cdot 10^{-4}$.

8. Cooling Rates

In this section, we estimate analytically the cooling rates which can be achieved with either the electron cooling or the stochastic cooling. We define the transverse and longitudinal cooling rate[4] with respect to the transverse emittance ϵ and the mean square momentum deviation δ^2, respectively,

$$\frac{1}{\tau_{tr}} = -\frac{1}{\epsilon}\frac{\mathrm{d}\epsilon}{\mathrm{d}t} \tag{73}$$

$$\frac{1}{\tau_{l}} = -\frac{1}{\delta^2}\frac{\mathrm{d}\delta^2}{\mathrm{d}t} \tag{74}$$

8.1 Electron Cooling

In Table 5 the parameters of the planned electron cooler are listed. The longitudinal and transverse cooling rates which can be achieved with magnetized electron cooling can be estimated using the formalism of Parkhomchuk [27, 28].

Table 5: Parameter of the electron cooler

Maximum Energy	4 MeV
Beta Function at Cooler	100 m
Cooling Section Length	30 m
Electron Beam Radius	5 mm
Electron Beam Current	1.0 A
Electron Beam Density	$2.7 \cdot 10^8$ cm^{-3}
Magnetic Field in Cooler	0.2 T
Field Homogeneity	$1 \cdot 10^{-5}$
Transverse Electron Temperature	0.1 eV

$$\frac{1}{\tau} = \frac{4\pi r_p r_e n_e c L_c L_{coul}}{\gamma^2 C}\frac{c^3}{v_{eff}^3}\frac{1}{1+(\epsilon/\epsilon_{eff})^{3/2}}. \tag{75}$$

Here, $r_p = 1.535 \cdot 10^{-18}$ m and $r_e = 2.818 \cdot 10^{-15}$ m is the classical proton and electron radius, n_e the electron density, L_c the length of the electron cooler, C the circumference, $L_{coul} \approx 10$ the Coulomb logarithm, $v_{eff} \approx 3 \cdot 10^4$ m/s an effective velocity representing the cooler's imperfections and ϵ_{eff} an effective emittance defined by

$$\epsilon_{eff} = \left(\frac{v_{eff}}{\beta\gamma c}\right)^2 \beta_c. \tag{76}$$

Here, β_c is the mean beta function in the region of the cooler. For very small transverse emittances the longitudinal and transverse cooling rate is inversely proportional to γ^2.

[4] Often, the cooling rates are defined with respect to the amplitudes $\sqrt{\epsilon}$ and δ. Then, the resulting cooling rates are a factor 1/2 smaller.

For large transverse emittances, i.e. $\epsilon \gg \epsilon_{eff}$, it is inversely proportional to γ^5 and $\epsilon^{3/2}$. It should be mentioned that transverse and longitudinal cooling rates are equal in the case of magnetized electron cooling. Thus, both cooling rates can be estimated using Eq. (75).

Concerning numerical results we refer to recent studies of Stockhorst [29] and Boine-Frankenheim [30]. Stockhorst investigates a scenario for the HR mode where the beam is injected into HESR at $T = 3$ GeV and precooled with the electron cooler. The beam-target interaction and IBS are taken into account. The resulting equilibrium values at 3 GeV are

$$\begin{aligned} \epsilon_{x,eq} &= 0.0024 \text{ mm mrad}, \\ \epsilon_{y,eq} &= 0.00063 \text{ mm mrad}, \\ \delta_{eq} &= 3.4 \cdot 10^{-5}. \end{aligned} \tag{77}$$

Then, the beam is accelerated to a kinetic energy of 8 GeV and again electron cooled. This yields the following equilibrium values

$$\begin{aligned} \epsilon_{x,eq} &= 0.0034 \text{ mm mrad}, \\ \epsilon_{y,eq} &= 0.00048 \text{ mm mrad}, \\ \delta_{eq} &= 3.0 \cdot 10^{-5}. \end{aligned} \tag{78}$$

Similar results have been obtained by Boine-Frankenheim [30].

8.2 Stochastic Cooling

The cooling rates which can be reached with stochastic cooling can be estimated using the formalism of Möhl et al. [31]. The cooling rate depends on the bandwidth W, the number N of particles in the ring, the gain factor g, the mixing factor M of the wanted mixing between successive pick-up's, the mixing factor $\tilde{M}$ of the unwanted mixing between observation and correction, i.e. pick-up and kicker, and the noise factor U. The gain factor g is defined as the fraction of the observed sample error corrected per turn. Ideally, $g = 1$, but in practice one adjusts $g < 1$. Due to the momentum spread, particles go round at slightly different speeds. Because of this mixing, the sample population changes. The dipersion of the revolution time T is given by

$$\frac{\Delta T}{T} = -\eta \frac{\Delta p}{p} \tag{79}$$

Here, η is the socalled frequency slip factor which is related to the Lorentz γ and the parameter γ_{tr} of the lattice,

$$\eta = \frac{1}{\gamma^2} - \frac{1}{\gamma_{tr}^2}. \tag{80}$$

Thus, η is not a constant, but depends on the beam energy. Below the transition energy, i.e. for $\gamma < \gamma_{tr}$, η is positive, above, it is negative. In the case of the HESR lattice, γ_{tr} is imaginary, $\gamma_{tr} = i6.5$ and η is allways positive. The resulting mixing factor M is defined as the number of turns for a particle with a momentum deviation of four standard deviations δ to migrate by one sample length. It can be estimated using

$$M = \frac{f}{2W} \frac{1}{4\delta|\eta|}. \tag{81}$$

Here, f is the revolution frequency and δ is the rms relative momentum spread of the beam. This equation shows that the mixing factor is not a constant, but it is inversely proportional to the momentary rms width δ of the beam. Thus, if longitudinal stochastic cooling is applied M is not constant but increases during the cool-down process since δ decreases. If only transverse cooling without any longitudinal cooling or heating is applied M stays constant during the cool-down process. In other words, the momentary

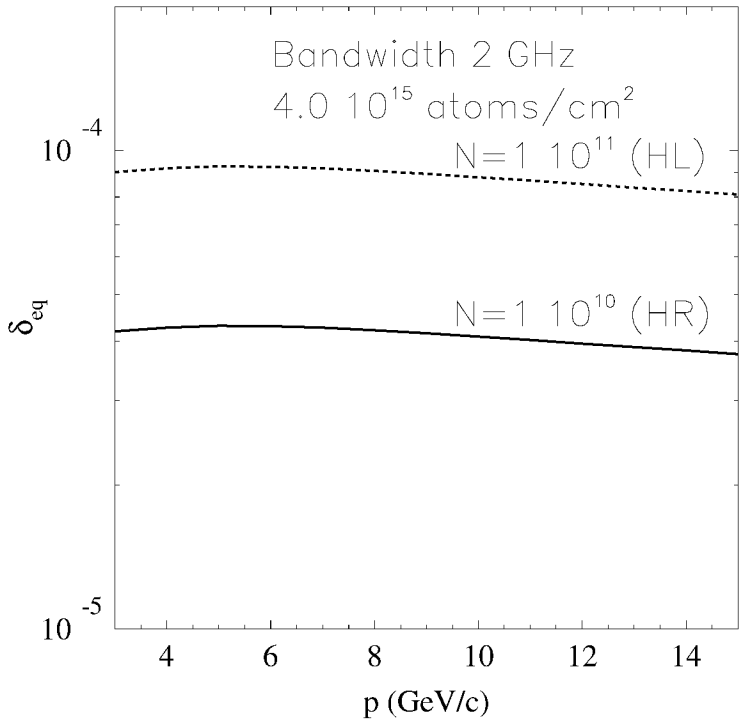

Fig. 19: Equilibrium rms momentum spread δ_{eq} vs. beam momentum p. The figure shows the equilibrium values which can be reached with a bandwidth of 2 GHz of a 2-4 GHz stochastic cooling system and $4 \cdot 10^{15}$ target atoms/cm^2. Since the longitudinal beam heating is dominated by the beam-target interaction IBS and other effects have been neglected. The assumed relative momentum acceptance $\delta_{cut} = 1 \cdot 10^{-3}$ refers to the standard mode of operation.

mixing factor M depends allways on the momentary rms width δ of the beam. The mixing factor $\tilde{M}$ is proportional to M,

$$\tilde{M} = M\frac{C}{L}. \tag{82}$$

Here, C/L denotes the ratio of the circumference to the distance L between pick-up and kicker. For the HESR we get $\tilde{M} = 2M$. Using these definitions, the transverse cooling rate may be written [31]

$$\frac{1}{\tau_{tr}} = \frac{W}{N}\left[2g\left(1 - \frac{1}{\tilde{M}^2}\right) - g^2(M+U)\right]. \tag{83}$$

The longitudinal cooling rate reads

$$\frac{1}{\tau_l} = 2\,\frac{W}{N}\left[2g\left(1 - \frac{1}{\tilde{M}^2}\right) - g^2(M+U)\right]. \tag{84}$$

The optimum gain factor is given by

$$g_{opt} = \frac{1-\tilde{M}^{-2}}{M+U}. \tag{85}$$

If the stochastic devices are cooled to liquid nitrogen temperature the noise factor is negligible, $U = 0$. Eqs. (83) and (84) can be further simplified by taking into account that the actual mixing factors are relatively large, i.e. $M \gg 1$ and $\tilde{M} \gg 1$. Taking also the condition (85) into account we then get the optimum gain factor g_{opt} and the optimum transverse and longitudinal cooling rates

$$g_{opt} = \frac{1}{M} = \frac{8W\delta|\eta|}{f}, \tag{86}$$

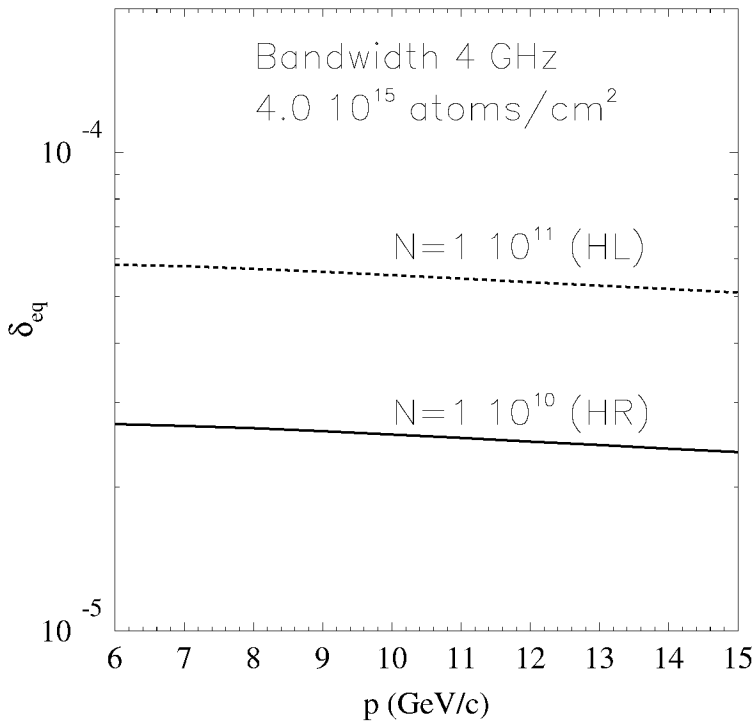

Fig. 20: Equilibrium rms momentum spread δ_{eq} vs. beam momentum p. The figure shows the equilibrium values which can be reached with a bandwidth of 4 GHz of a 4-8 GHz stochastic cooling system and $4 \cdot 10^{15}$ target atoms/cm^2. Since the longitudinal beam heating is dominated by the beam-target interaction IBS and other effects have been neglected. The assumed relative momentum acceptance $\delta_{cut} = 1 \cdot 10^{-3}$ refers to the standard mode of operation.

$$\frac{1}{\tau_{tr}} = 8\,\frac{W^2|\eta|\delta}{N\,f}, \tag{87}$$

$$\frac{1}{\tau_{l}} = 16\,\frac{W^2|\eta|\delta}{N\,f}. \tag{88}$$

In the case of longitudinal stochastic cooling, the resulting equilibrium value δ_{eq} can be estimated by inserting τ_l into Eq. (71),

$$\delta_{eq}^2 = \delta_{rms}^2 f \frac{Nf}{16W^2|\eta|\delta_{eq}}. \tag{89}$$

Solving for δ_{eq} yields

$$\delta_{eq} = \left(\frac{\delta_{rms}^2 f^2 N}{16W^2|\eta|}\right)^{1/3}. \tag{90}$$

The coresponding optimum gain factor g_{eq} reads

$$g_{eq} = \frac{1}{M_{eq}} = \frac{8W\delta_{eq}|\eta|}{f}. \tag{91}$$

The resulting cooling rate may be calculated by inserting δ_{eq} into Eq. (88). The equilibrium value δ_{eq} can be reached by adjusting the corresponding optimum gain g_{eq}, see Eq. (91). It takes the beam-target interaction fully into account. The beam-target effects are represented by the term δ_{rms}^2, i.e. the mean square momentum deviation per target traversal. It is interesting to note that δ_{eq} is proportional to $N^{1/3}$,

$f^{2/3}$, $\delta_{rms}^{2/3}$ and inversely proportional to $W^{2/3}$ and $|\eta|^{1/3}$. We repeat that this holds true, provided the mixing factors are very large, i.e. $M \gg 1$ and $\tilde{M} \gg 1$.

Table 6: Longitudinal cooling rates $1/\tau_l$ and δ_{eq} for $N = 1 \cdot 10^{10}$ (HR), $\delta_{cut} = 1 \cdot 10^{-3}$ and $4 \cdot 10^{15}$ atoms/cm^2

T (GeV)	δ_{rms}^2	f (MHz)	$1/\tau_l$ (s^{-1})	δ_{eq}
2.0	$2.38 \cdot 10^{-16}$	0.4949	0.0677	$4.2 \cdot 10^{-5}$
4.0	$1.15 \cdot 10^{-16}$	0.5128	0.0321	$4.3 \cdot 10^{-5}$
6.0	$7.78 \cdot 10^{-17}$	0.5175	0.0221	$4.3 \cdot 10^{-5}$
8.0	$5.91 \cdot 10^{-17}$	0.5194	0.0178	$4.2 \cdot 10^{-5}$
10.0	$4.78 \cdot 10^{-17}$	0.5204	0.0154	$4.0 \cdot 10^{-5}$
12.0	$4.01 \cdot 10^{-17}$	0.5209	0.0138	$3.9 \cdot 10^{-5}$
14.0	$3.46 \cdot 10^{-17}$	0.5213	0.0128	$3.8 \cdot 10^{-5}$

Table 7: Longitudinal cooling rates $1/\tau_l$ and δ_{eq} for $N = 1 \cdot 10^{11}$ (HL), $\delta_{cut} = 1 \cdot 10^{-3}$ and $4 \cdot 10^{15}$ atoms/cm^2

T (GeV)	δ_{rms}^2	f (MHz)	$1/\tau_l$ (s^{-1})	δ_{eq}
3.0	$1.54 \cdot 10^{-16}$	0.5072	0.0093	$9.2 \cdot 10^{-5}$
4.0	$1.15 \cdot 10^{-16}$	0.5128	0.00691	$9.3 \cdot 10^{-5}$
6.0	$7.78 \cdot 10^{-17}$	0.5175	0.00477	$9.2 \cdot 10^{-5}$
8.0	$5.91 \cdot 10^{-17}$	0.5194	0.00383	$9.0 \cdot 10^{-5}$
10.0	$4.78 \cdot 10^{-17}$	0.5204	0.00331	$8.7 \cdot 10^{-5}$
12.0	$4.01 \cdot 10^{-17}$	0.5209	0.00298	$8.4 \cdot 10^{-5}$
14.0	$3.46 \cdot 10^{-17}$	0.5213	0.00275	$8.1 \cdot 10^{-5}$

Now we like to estimate the equilibrium values δ_{eq} and the cooling rates corresponding to the equilibrium for the HR and HL mode which differ by the number of particles in the ring, $N = 1 \cdot 10^{10}$ (HR) and $N = 1 \cdot 10^{11}$ (HL), respectively. The planned stochastic cooling system [32] works in the frequency range 2-4 GHz. For $N = 1 \cdot 10^{10}$ (HR mode) it can be used in the kinetic energy range $T > 1.5$ GeV. For $N = 1 \cdot 10^{11}$ (HL mode) it can be used in the kinetic energy range $T > 3.0$ GeV. Below those thresholds it cannot be used since there is overlap of the revolution bands of adjacent harmonics [32]. We assume the following parameters for the HESR ring and the planned stochastic cooling system, $\gamma_{tr} = i\,6.5$ and $W = 2$ GHz. In the calculation one must take the energy dependence of η (see Eq. (80)) into account. In Tables 6 and 7 the resulting cooling rates $1/\tau_l$ and equilibrium values δ_{eq} are listed for several beam momenta. In Fig. 19 the equilibrium values δ_{eq} are plotted as a function of the beam momentum. The resulting equilibrium values δ_{eq} are nearly independent of the beam momentum. In the HR mode $\delta_{eq} \approx 4 \cdot 10^{-5}$ can be achieved, in the HL mode $\delta_{eq} \approx 9 \cdot 10^{-5}$. These values are in agreement with a recent evaluation by Stockhorst [32] who gets also values of about $4 \cdot 10^{-5}$ for the HR mode at 4 and 8 GeV. It should be mentioned that a 4–8 GHz longitudinal stochastic cooling system with a bandwidth of 4 GHz would improve the final momentum resolution by a factor $2^{2/3}$, see Eq. (90). Thus, a relative momentum spread $\delta_{eq} \approx 2.5 \cdot 10^{-5}$ for the HR mode and $\delta_{eq} \approx 5.7 \cdot 10^{-5}$ for the HL mode could be reached, see Fig. 20. But such a system could only be used for kinetic energies $T > 5$ GeV due to the band overlap of adjacent harmonics [32].

It should be pointed out that Eqs. (87) and (88) have been derived assuming the optimum gain factor as given by Eq. (85). That means that the gain g_{opt} must be changed continuously during the cool-down process, since δ decreases, see Eq. (86). But in practice, a constant gain factor is adjusted. Thus,

in order to reach the highest momentum resolution, i.e. the equilibrium value δ_{eq} as given by Eq. (90), one should choose a priori the gain factor g_{eq} corresponding to δ_{eq}, see Eq. (91).

8.3 Comparison of electron and stochastic cooling

The actual studies of electron and stochastic cooling show that both methods fail to reach the original goal of the HR mode, a momentum resolution corresponding to $\delta_{eq} = 1 \cdot 10^{-5}$. Nevertheless, both methods achieve a momentum resolution which is not far away from the original goal. Electron cooling yields $\delta_{eq} \approx 3 \cdot 10^{-5}$, stochastic cooling with a bandwidth of 2 GHz yields $\delta_{eq} \approx 4 \cdot 10^{-5}$ and stochastic cooling with a bandwidth of 4 GHz yields $\delta_{eq} \approx 2.5 \cdot 10^{-5}$. But electron cooling has several severe disadvantages compared to stochastic cooling.

The problem of the electron cooling is the fact that the transverse cooling is so strong that extremely small transverse emittances result. As a consequence, the transverse and longitudinal heating rates due to IBS are extremely large, much larger than the corresponding heating rates due to the beam-target interaction. As a consequence, the longitudinal heating rate due to IBS is so strong that $\delta_{eq} = 1 \cdot 10^{-5}$ cannot be reached. Another negative consequence of the small transverse emittances is the very high beam loss rate due to the Touschek effect which affects the average luminosity.. Furthermore, the beam spot at the target point is much too small. The transverse beam width at the target is given by

$$\begin{aligned} \sigma_x &= \sqrt{\beta_x \epsilon_x}, \\ \sigma_y &= \sqrt{\beta_y \epsilon_y}. \end{aligned} \tag{92}$$

Taking the equilibrium emittances at 8 GeV as quoted in Eq. (78) one gets with $\beta_x = \beta_y = 1$ m at the target

$$\begin{aligned} \sigma_x &= 0.058 \text{ mm}, \\ \sigma_y &= 0.022 \text{ mm}. \end{aligned} \tag{93}$$

In a scenario where the pellet target is used beam spots with $\sigma_{x,y} = 1$ mm are needed in order to have sufficient overlap between beam and target. The beam spot area noted in Eq. (93) is a factor of 800 too small.

The great advantage of the stochastic cooling is the fact that the transverse and longitudinal cooling rates can be adjusted independently. It is even possible to adjust the gain factors such that the beam is longitudinally cooled and transversely heated. The cooling rate in Eq. (83) gets negative, i.e. becomes a heating rate if the second term in Eq. (83) is larger than the first term. Thus, it is possible to adjust individually $1/\tau_x$, $1/\tau_y$ and $1/\tau_l$. A possible mode of operation is to cool down longitudinally right from the start in order to reach δ_{eq} as fast as possible. Simultaneously, $1/\tau_x$ and $1/\tau_y$ are first adjusted such that $(\epsilon_x)_{\text{start}} \rightarrow 1$ mm mrad and $(\epsilon_y)_{\text{start}} \rightarrow 1$ mm mrad. Then, $1/\tau_x$ and $1/\tau_y$ are adjusted to maintain the equilibrium values $\epsilon_{x,eq} = 1$ mm mrad and $\epsilon_{y,eq} = 1$ mm mrad.

9. Summary and Conclusions

The beam-target interaction has been studied with respect to the beam heating processes by internal targets in the HESR ring. The transverse and longitudinal heating rates can be evaluated using analytic expressions. The transverse emittance growth is determined by the mean square scattering angle Θ^2_{rms} per target traversal. The longitudinal emittance growth, more precisely the growth of the mean square relative momentum deviation δ^2 of the beam, is determined by the mean square relative momentum loss δ^2_{rms} per target traversal which is related to the energy loss straggling $\Delta\epsilon^2_{rms}$. An important result is the

fact that the growth rate of δ^2 can be kept an order of magnitude smaller by cutting the long tails of the energy loss distribution.

The study of the beam-target interaction includes a comparison with the important beam heating processes which are due to IBS. To this end the longitudinal and transverse IBS heating rates are evaluated using analytic expressions. The heating rates due to IBS depend strongly on the transverse emittances. Fortunately, IBS beam heating can be kept small by adjusting rather large equilibrium emittances of about 1 mm mrad. Then, the IBS heating rates are small compared to the beam-target heating rates. But equilibrium emittances of about 0.001 mm mrad which are typical for electron cooled beams yield tremendous transverse and longitudinal IBS heating rates which are very much larger than the beam-target heating rates.

An important point of the beam-target interaction is the question of beam losses. It turns out that the main beam losses are due to the total cross section of the hadronic $\bar{p}p$ interaction. The next most important loss rate is due to the restricted momentum acceptance of the ring, i.e. the cutting of the long tails of the energy loss distribution. The losses due to the large angle Coulomb scattering in the target can be kept negligibly small if a transverse acceptance angle $\Theta_{cut} \approx 4$ mrad is chosen. The same holds true for the losses due to the Touschek effect if equilibrium emittances of about 1 mm mrad are adjusted. However, the Touschek losses become very large for equilibrium emittances of about 0.001 mm mrad which are typical for electron cooled beams.

Using the total loss rate and assuming a production rate of $8 \cdot 10^6$ antiprotons/s, the maximum possible average luminosity $\bar{L}$ has been evaluated as a function of the beam momentum p. The average luminosity $\bar{L}$ is proportional to the antiproton production rate $\mathrm{d}N_{prod}/\mathrm{d}t$ and the mean lifetime of the beam, i.e. the time constant τ_{loss}. It turns out that the maximum average luminosity $\bar{L}$ is in the range $0.37 \cdot 10^{32} - 1.05 \cdot 10^{32}$ cm^{-2}s^{-1} if the antiprotons at the end of each cycle are recycled. Dumping the antiprotons at the end of each cycle yields average luminosities between $0.17 \cdot 10^{32}$ and $0.48 \cdot 10^{32}$ cm^{-2}s^{-1}. The values are shown in Figs. 15 and 16. The resulting maximum average luminosities are more than a factor of two smaller than the original goal of $2.0 \cdot 10^{32}$ cm^{-2}s^{-1} which was foreseen for the HL mode. This is due to the fact that the antiproton production rate has been reduced in stage 1 from the original value of $2 \cdot 10^7$ s^{-1} to $8 \cdot 10^6$ s^{-1}. The design luminosity of $2.0 \cdot 10^{32}$ cm^{-2}s^{-1} can be achieved in a later stage by upgrading the antiproton production rate.

The equilibrium between beam cooling and beam heating is discussed. Expressions are derived in order to evaluate the transverse cooling rates $1/\tau_{tr}$ which are needed in order to maintain certain transverse emittances ϵ_{eq}. Similarly, expressions are derived in order to evaluate the longitudinal cooling rates $1/\tau_l$ which are needed in order to reach certain momentum resolutions, more precisely the corresponding equilibrium values of the relative rms momentum spread δ_{eq}. Equilibrium values are deduced assuming that the beam-target effects are dominating. Numerical results are shown as a function of the beam momentum for the HR and HL mode assuming a *standard mode of operation* with equilibrium emittances $\epsilon_{eq} = 1$ mm mrad, maximum scattering angles $\Theta_{cut} = 4$ mrad and a relative momentum acceptance $\delta_{cut} = 1 \cdot 10^{-3}$.

The cooling rates which can be achieved with electron cooling are discussed. The electron cooling rates can be estimated analytically using the formalism of Parkhomchuk for magnetized electron cooling. Recent studies of electron cooling by Stockhorst [29] and Boine-Frankenheim [30] show that a momentum resolution corresponding to $\delta_{eq} \approx 3 \cdot 10^{-5}$ can be achieved for the HR mode. But the drawback of electron cooling is the fact that very small transverse equilibrium emittances $\epsilon_{eq} \approx 0.001$ mm mrad evolve. As a consequence, the transverse and longitudinal heating rates due to IBS and the Touschek loss rates become very high and the target beam spot is about a factor of 800 too small compared to what is needed for the pellet target.

The stochastic cooling rates can be estimated analytically using the formalism of Möhl et al. [31]. The optimum gain factor depends on the mixing factors M and $\tilde{M}$. It turns out that in the case of HESR the mixing factors are rather large. This fact has been used in order to derive a simple expression which

allows to calculate the optimum momentum resolution, i.e. the minimum momentum spread δ_{eq} which can be achieved with stochastic cooling. It turns out that a stochastic cooling system with a bandwidth of 2 GHz yields a relative rms momentum spread of about $4 \cdot 10^{-5}$ for the HR mode and about $9 \cdot 10^{-5}$ for the HL mode. It is interesting to note that stochastic cooling with a bandwidth of 4 GHz would yield relative rms momentum spreads of about $2.5 \cdot 10^{-5}$ (HR) and $5.7 \cdot 10^{-5}$ (HL), respectively, for the kinetic energy range $T > 5$ GeV. The great advantage of the stochastic cooling is the fact that the horizontal, vertical and longitudinal cooling rates can be adjusted individually. Thus, it is possible to adjust transverse emittances of 1 mm mrad as required by the experiment and to reach simultaneously high momentum resolutions.

ACKNOWLEDGEMENTS

I would like to thank Oliver Boine-Frankenheim, Andreas Lehrach, Rudolf Maier, Dieter Prasuhn, Hans Stockhorst, Pavel Zenkevich and Volker Ziemann for helpful informations and discussions.

References

[1] An International Accelerator Facility for Beams of Ions and Antiprotons, Conceptional Design Report, GSI Darmstadt, November 2001, see http://www.gsi.de/GSI-Future/cdr/.

[2] FAIR Project (subproject HESR), Technical Report, to be published in 2005.

[3] Strong Interaction Studies with Antiprotons, Letter of Intent, PANDA Collaboration, January 2004, see http://www.gsi.de/documents/DOC-2004-Jan-115-1.pdf.

[4] Antiproton-Proton Scattering Experiments with Polarization, Letter of Intent, PAX Collaboration, January 2004, see http://www.gsi.de/documents/DOC-2004-Jan-125-1.pdf.

[5] F. Rathmann et al., A Method to Polarize Stored Antiprotons to a High Degree, Phys. Rev. Lett. **94** (2005) 014801.

[6] A Study of Spin-dependent Interactions with Antiprotons, Letter of Intent, ASSIA Collaboration, January 2004, see http://www.gsi.de/documents/DOC-2004-Jan-152-1.pdf.

[7] P. Sigmund and K. B. Winterbon, Nucl. Instr. and Meth. **119** (1974) 541.

[8] F. Hinterberger and D. Prasuhn, Nucl. Instr. and Meth. **A279** (1989) 413.

[9] Particle Data Group, Phys. Rev. D **66**, 010001-1 (2002).

[10] G. Molière, Z. Naturforsch. **2a** (1947) 133.

[11] G. Molière, Z. Naturforsch. **3a** (1948) 78.

[12] U. Fano, Phys. Rev. **93** (1954) 117.

[13] B. Rossi and K. Greisen, Rev. Mod. Phys. **13** (1941) 240.

[14] L. Landau, J. Phys. USSR **8** (1944) 201.

[15] P. V. Vavilov, Soviet Physics JETP **5** (1957) 749.

[16] F. Hinterberger, T. Mayer-Kuckuk and D. Prasuhn, Nucl. Instr. and Meth. in Phys. Res. **A275** (1989) 239.

[17] A. Piwinski, Proc. 9th Int. Conf. on High Energy Accelerators, p.105 (1974) and CERN Report **85-19** 451 (1985).

[18] A. H. Sørensen, CERN Report **87-10** (1987) 135.

[19] J. D. Bjorken and S. K. Mtingwa, Part. Acc. **13** (1983) 115.

[20] A. Fedotov, BNL Report C-A/AP **168** (2004).

[21] M. Martin, CERN Report **PS/84-9 (AA)** (1984).

[22] http://pdg.lbl.gov/2004/hadronic-xsections/hadron.html.

[23] S. Eidelman et al., Phys. Lett. B592,1 (2004).

[24] V. A. Lebedev, J. S. Hangst, N. Madsen and A. Labrador, Nucl. Instr. and Meth. A **391** (1997) 176.

[25] A. Lehrach, O. Boine-Frankenheim, F. Hinterberger, R. Maier and D. Prasuhn, Beam Performance and Luminosity Limitations in the High-Energy Storage Ring (HESR), Proceedings of the High Intensity Beam Dynamics-Coulomb05 Workshop, Senigallia, Italy (2005), accepted for publication in Nucl. Instr. and Meth. in Phys. Res. A.

[26] F. Hinterberger, Talk at PANDA Meeting in Darmstadt, Sept. 2005.

[27] V. V. Parkhomchuk, Nucl. Instr. and Meth. in Phys. Res. A **441** (2000) 9.

[28] O. Boine-Frankenheim, R. Hasse, F. Hinterberger and P. Zenkevich, submitted for publication in Nucl. Instr. and Meth. in Phys. Res. A.

[29] H. Stockhorst, Electron and Stochastic Cooling Investigations for the HESR, 12th HESR-Consortium Meeting at TSL, Uppsala, June 16th, 2005.

[30] O. Boine-Frankenheim, Talk at FZ Jülich, August 2005.

[31] D. Möhl et al., Phys. Rep. 58 (1980), D. Möhl, CERN Report **84-15** (1984).

[32] H. Stockhorst, Design Deliberations for a Stochastic Cooling System at HESR -High Resolution and High Luminosity Mode Performance-, 19. 10. 2005, Version 2 and private communication.

Forschungszentrum Jülich
in der Helmholtz-Gemeinschaft

Jül-4206
Februar 2006
ISSN 0944-2952